Theta and alpha power track the acquisition and reversal of threat predictions and correlate with skin conductance response

Theta and alpha power track the acquisition and reversal of threat predictions and correlate with skin conductance response

Starita F. [1*], Pirazzini G. [2], Ricci G. [2], Garofalo S. [1], Dalbagno D. [1], Degni L.A.E. [1], di Pellegrino G. [1], Magosso E. [2], Ursino M.[2]

[1] Center for Studies and Research in Cognitive Neuroscience, Department of Psychology, University of Bologna, 40126, Bologna, Italy

[2] Department of Electrical, Electronic, and Information Engineering "Guglielmo Marconi", University of Bologna, 47521, Cesena, Italy

Corresponding author: Francesca Starita

Address: Viale Rasi e Spinelli, 176, 47521 Cesena FC

Phone: +39 339 3948076

Email: francesca.starita2@unibo.it

Abstract

The ability to flexibly adjust one's threat predictions to meet the current environmental contingencies is crucial to survival. Nevertheless, its neural oscillatory correlates remain elusive in humans. Here, we tested whether changes in theta and alpha brain oscillations mark the updating of threat predictions and correlate with response of the peripheral nervous system. To this end, electroencephalogram and electrodermal activity were recorded in a group of healthy adults, who completed a Pavlovian threat conditioning task that included an acquisition and a reversal phase. Both theta and alpha power discriminated between threat and safety, with each frequency band showing unique patterns of modulations during acquisition and reversal. While changes in midcingulate theta power may learn the timing of an upcoming danger, alpha power may reflect the preparation of the somato-motor system. Additionally, ventromedial prefrontal cortex theta may play a role in the inhibition of previously acquired threat responses, when they are no longer appropriate. Finally, theta and alpha power correlated with skin conductance response, establishing a direct relationship between activation of the central and peripheral nervous systems. Taken together these~~our~~ results highlight the existence of multiple oscillatory systems that flexibly regulate their activity for the successful expression of threat responses in an ever-changing environment.

Accurately predicting impending danger is crucial to survival. Additionally, the ability to flexibly readjust one's predictions to meet the current environmental contingencies is equally adaptive, especially in an ever-changing environment. Indeed, failing to realize that an initially dangerous stimulus is now a cue for safety may be as costly as the alternative, and the consequences of such failure are evident in a number of anxiety-related disorders, characterized by persistence of threat responses even when they are no longer needed (Duits et al., 2015). Such flexibility of threat predictions can be reliably studied through reversal learning paradigms. In these tasks, after an initial acquisition phase in which participants learn that one stimulus predicts an aversive outcome while another stimulus does not, stimulus-outcome contingencies are reversed. The previously safe stimulus now becomes the threatening one, while the threatening stimulus is now the safe one. Importantly, acquisition and reversal are distinct processes. While acquisition mainly requires the development of a threat response to the shock-predicting stimulus, reversal involves greater cognitive control, requiring the simultaneous inhibition and development of the threat response, as the threat response previously acquired to one stimulus must be inhibited and targeted elsewhere (Schiller et al., 2008; Schiller & Delgado, 2010).

Brain rhythms have been identified as a neurophysiological mechanism suitable for the study of prediction acquisition and updating (Arnal & Giraud, 2012; Tarasi et al., 2022), and theta and alpha oscillations appear to play a role in the initial acquisition and subsequent recall of threat predictions (Bierwirth et al., 2021; Mueller et al., 2014; Panitz et al., 2019; Sperl et al., 2019; Yin et al., 2020). Nevertheless, in humans, no study, to our knowledge, has investigated how brain rhythms change from the initial acquisition to the subsequent reversal of threat predictions.

In this regard, midcingulate theta frequency (4-8Hz) oscillations show increased power during the recall of previously acquired threat predictions (Bierwirth et al., 2021; Mueller et al., 2014; Sperl et al., 2019). Additionally, medial prefrontal cortex (mPFC) theta, including its more ventral portion, shows increased power to the presentation of stimuli predicting an aversive outcome, relative to control, during the acquisition of threat predictions (Chen et al., 2021). Indeed, the ventral mPFC is known to have a crucial role in the acquisition, extinction and reversal of threat predictions (Battaglia et al., 2020; Fullana et al., 2016, 2018; Morris & Dolan, 2004; Phelps et al., 2004; Savage et al., 2020; Schiller et al., 2008; Schiller & Delgado, 2010). Besides threat learning, increase in midcingulate theta power has been observed in response to novelty, conflict (including in task switching) and error commission (Cavanagh et al., 2010, 2013; Hajihosseini & Holroyd, 2013), such that changes in theta power have been suggested as a mechanism for the implementation of cognitive control (Cavanagh & Frank, 2014). Additionally, stimulation of the frontal cortex at theta frequency has been shown to fasten reversal learning in a gambling task (Wischnewski et al., 2016). Given this evidence, theta oscillations may have a crucial role not only in the initial acquisition of threat predictions, but also in the regulation of their expression/inhibition, critical for successful reversal.

Changes in alpha (8-14Hz) frequency oscillations of sensory cortical networks have also been implicated in threat predictions. For example, decreased alpha power over occipital electrodes has been found in response to visual conditioned stimuli, during the initial acquisition (Yin et al., 2020) and subsequent recall (Panitz et al., 2019) of threat learning. Also, greater alpha desynchronization at somato-motor electrode sites has been found in anticipation of painful somatosensory stimuli (Babiloni et al., 2003, 2008, 2010, 2014). More broadly, alpha oscillations have been proposed to convey top-

down sensory predictions (Mayer et al., 2016; Tarasi et al., 2022), and may thus be crucial to enable enhanced sensory processing of cues associated with danger often observed during threat learning (Miskovic & Keil, 2012; Riels et al., 2022).

In addition to changes in the response of the central nervous system, threat learning is known to elicit consistent responses of the autonomic nervous system (Lonsdorf et al., 2017). Among these, the skin conductance response is the most widely assessed (Bach et al., 2010; Beckers et al., 2013; Lonsdorf et al., 2019; Ojala & Bach, 2020; Sjouwerman & Lonsdorf, 2019), with extensive literature showing that the increase in skin conductance response for conditioned stimuli is a robust conditioned response, evident both during threat learning acquisition (Bach et al., 2010; Lonsdorf et al., 2017) and reversal (Schiller et al., 2008). Nevertheless, the relationship between changes in skin conductance and brain rhythms during threat learning remains open for investigation. Indeed, a negative correlation has been shown between mean alpha power and skin conductance level, at rest, such that alpha has been proposed to be an arousal measure (Barry et al., 2007). Whether a similar relationship exists also when anticipating the arrival of an aversive outcome, and whether it pertains also the theta rhythm, remains to be investigated.

Given this evidence, ~~we~~ the aim of this study is to identify whether and how changes in theta and alpha brain oscillations track the acquisition and reversal of threat learning. To this end, electroencephalogram was recorded in a group of healthy adults, who completed a Pavlovian threat conditioning task that included an acquisition and a reversal phase. During acquisition, participants learned to identify a visual stimulus (A) as threatening, i.e. conditioned stimulus (CS+), while another stimulus (B) served as within-subject control condition (CS-). Thus, presentation of the CS+ co-terminated with the delivery of an aversive shock (i.e. unconditioned stimulus, US) in 50% of the trials, while presentation of the CS- never terminated with shock. During reversal, the contingencies were reversed, such that stimulus A was now the new CS- (old CS+) and stimulus B the new CS+ (old CS-).

An analysis at the level of cortical sources, reconstructed from the EEG signals, was performed to investigate theta and alpha rhythms in some key regions of interest (ROIs), in particular of the left hemisphere (contralateral to the side of shock delivery), according to the previous description. We tested whether the acquisition of threat learning induced an increase in midcingulate and ventral mPFC theta power (Bierwirth et al., 2021; Chen et al., 2021; Mueller et al., 2014; Sperl et al., 2019) and a decrease in occipital, somatosensory, and motor alpha power to CS+ relative to CS-, as the CS+ becomes predictive of the US (Babiloni et al., 2003, 2008, 2010, 2014; Panitz et al., 2019; Riels et al., 2022; Yin et al., 2020). Because previous studies found that the difference between CS+ and CS- in theta power varied during the time course of CS presentation (Quirk & Mueller, 2008; Sperl et al., 2019), we also assessed the temporal evolution of changes in power during CS presentation. Additionally, we tested whether the changes in theta and alpha power are similar between acquisition and reversal or whether reversal is characterized by unique power modulations. Finally, during the task, electrodermal activity was also recorded serving two purposes. The first was to have a peripheral measure of threat learning acquisition and reversal. The second was to test the correlation between changes in neural response, i.e. theta and alpha, and psychophysiological response during acquisition and reversal.

Methods

Participants

Twenty right-handed healthy participants took part in the study. One participant did not complete the experimental session due to fainting. Thus, nineteen participants completed the study (8 males; age M = 23.48 years, SD = 1.85 years). The study followed the American Psychological Association Ethical Principles of Psychologists and Code of Conduct and the Declaration of Helsinki and was approved by the Bioethics Committee of the University of Bologna (Protocol number 71559). All participants provided written informed consent to participation.

Pavlovian threat acquisition and reversal task. Figure 1 illustrates the experimental task. Two different Japanese hiragana served as visual stimuli (Starita, Pietrelli, et al., 2019; Starita & di Pellegrino, 2018). During acquisition, participants learned to identify one hiragana (hiragana A) as dangerous, i.e. threat conditioned stimulus (CS+), while the other (hiragana B) served as within-subject control condition (CS-). Thus, presentation of the CS+ co-terminated with the delivery of an aversive shock (i.e. unconditioned stimulus, US) in 50% of the trials, while presentation of the CS- never terminated with shock. During reversal, the contingencies were reversed, such that hiragana A was now the new CS- (old CS+) and hiragana B the new CS+ (old CS-). Hiragana assignment to each CS role was counterbalanced between participants.

The US consisted of a 2ms aversive electrical shock (Effting & Kindt, 2007; Krypotos et al., 2014, 2015; Starita et al., 2022; Stemerding et al., 2022) generated by a Digitimer Stimulator (Model DS7A, Digitimer Ltd., UK) and delivered to the participants' right wrist through pre-gelled Ag/AgCl snapped electrodes (Friendship Medical, SEAg-S-15000/15x20). The US intensity (M = 43.47mA, SD = 22.41mA) was calibrated for each participant to a level deemed "highly unpleasant, but not painful" using an ascending staircase procedure (Lonsdorf et al., 2017; Starita et al., 2016, 2022; Starita, Kroes, et al., 2019). Participants rated the unpleasantness of the shock on a scale ranging from 0 (no sensation) to 10 (painful). Given that habituation to the US may be an issue due to the high number of experimental trials (Sperl et al., 2016), the unpleasantness of the shock rating was repeated before the beginning of each block (block 1 M=8.00, SD=0.47; block 2 M=7.79, SD=0.71; block 3 M=7.63, SD=1.07; block 4 M=7.47, SD=1.17). A one-way ANOVA on the ratings was conducted to test whether shock unpleasantness decreased over blocks; this showed no significant effect of block (p=0.147).

A computer running the OpenSesame software (Mathôt et al., 2012) controlled the flow of the task (Garofalo et al., 2020). On each trial, one hiragana appeared in the center of the computer screen (23.6 inches; resolution: 1440 x 900; refresh rate: 75 Hz). The task was divided into four blocks: acquisition 1 (Acq1), acquisition 2 (Acq2), reversal 1 (Rev1), reversal 2 (Rev2), and a pause of 5min was taken between each block. Each block included 40 trials (20 trials per CS) and each CS was presented for 6s followed by a jittered 11-14s inter-trial interval. Except for the first two acquisition trials that started with one CS- trial and one reinforced CS+ trial, in random order, trials proceeded in pseudo-random order, such that no more than two consecutive stimuli of the same type occurred in a row.

At the beginning of each block, participants read the following instructions: "You will see two different images, which will appear one at a time on the screen. Occasionally, the image may shock you. Your job is to figure out which image shocks you. Press any key to start." Note that no information was provided regarding which image would be associated with the shock, and participants had to learn the CS-US relationship from experience. Skin conductance and electroencephalogram were continuously

recorded during each block. At the end of each block, participants completed subjective ratings of CS valence, shock expectancy, and awareness of the CS-US contingencies (see dependent variables).

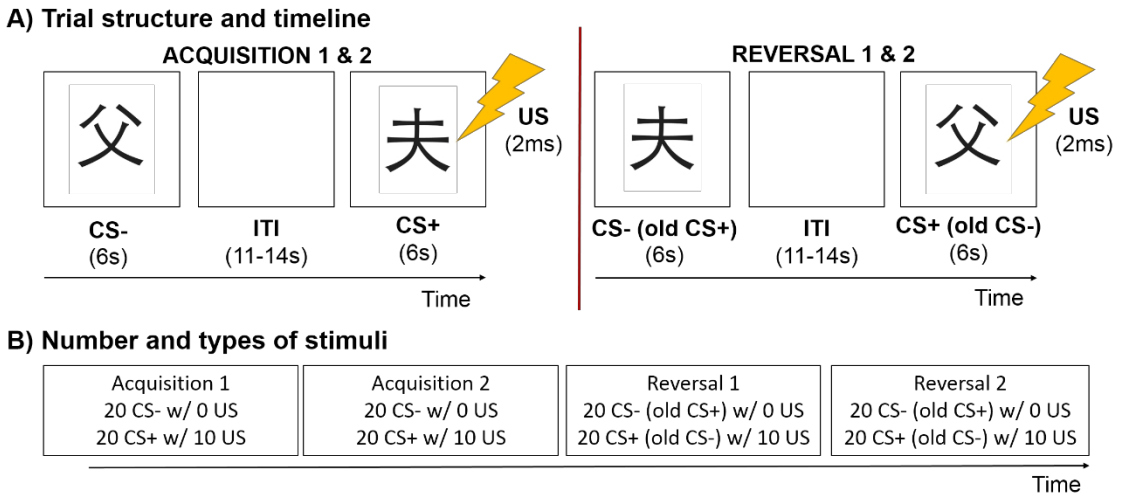

Figure 1. Pavlovian threat acquisition and reversal task. (A) Trial structure and timeline. All CSs were presented for 6s, followed by a jittered 11-14s intertrial interval. During acquisition and reversal, presentation of CS+ co-terminated with an aversive electric shock unconditioned stimulus (US, of 2ms duration) delivered at 6s. Note that during reversal, CS-US contingencies reversed relative to acquisition, such that the CS- corresponded to the old CS+ and the CS+ corresponded to the old CS-. (B) Number and types of stimuli presented during the task. Each acquisition and reversal block included 20 CS+ and 20 CS-. During each block, the CS+ was reinforced with an aversive US on 10 trials ("w/ 10", reinforcement rate of 50%), while the CS- was never paired with a US ("w/ 0").

Skin conductance response (SCR). Galvanic skin conductance was recorded during each block at 1000 Hz (gain switch set to 5, low-pass to 10 Hz), from pre-gelled snap electrodes (BIOPAC EL501) placed on the hypothenar eminence of the palmar surface of the left non-shocked hand, connected to a BIOPAC MP-150 System (Goleta, CA). The digitalized signal was down sampled at 200 Hz and processed using Autonomate 2.8 (Green et al., 2014) to obtain trough-to-peak SCR values. The Autonomate software identifies the trough and peak of candidate SCRs by locating zero crossings in the first-order temporal derivative of the downsampled data. A SCR was considered valid if the trough-to-peak deflection started between 0.5–4.5 s following the CS onset, lasted for a maximum of 5 s, and was greater than 0.02 μS. Trials that did not meet these criteria were scored as zero and remained in the analyses (Starita et al., 2016; Starita, Kroes, et al., 2019). Given that trough-to-peak deflection had to start before the time of shock delivery (6s) all shocked and non-shocked trials were included in the analysis. This is because any peak generated in response to the shock would start outside the window of CS-evoked SCR. In fact, to determine if candidate SCRs are likely to contain multiple overlapping responses (e.g. overlapping CS- and US-evoked SCR), inflection points are identified in the downsampled data by identifying zero crossings in the second-order temporal derivative. If the slope cycles from increasing to decreasing twice within one candidate SCR, then the overlapping responses are segmented at the inflection point where the slope changes from decreasing to increasing (in the middle of the rise) (Green et al., 2014). Following the automated analysis, all peaks were visually inspected to ensure correct peak scoring, and in case of erroneous scoring, the correct peak was manually defined. In order to reduce the impact of individual differences in skin conductance response, within-participant z-scoring was performed on the raw SCRs across the four experimental blocks (Boucsein et al., 2012; Lykken & Venables, 1971). Mean SCRs to CS+ and CS- were analyzed to verify threat conditioning acquisition.

Explicit CS-US contingency awareness. To evaluate explicit conditioning of the CS-US contingency, at the end of each block, participants saw each CS in random order and answered the question "In this block, this image shocked me", on an 11-point Likert scale ranging from 0 (never) to 10 (always).

Explicit ratings of CSs valence. To have an explicit measure of the subjective experience of CSs, at the end of each block, participants saw each CS in random order and answered the question "In this block, the feeling I had when seeing this image was", on an 11-point Likert scale ranging from 0 (unpleasant) to 10 (pleasant), with 5 (neutral).

EEG recording and processing. The EEG was recorded with Ag/AgCl electrodes (Fast n Easy Electrodes, Easycap, Herrsching, Germany) from 63 electrode sites (Fp1, Fp2, AF3, AF4, AF7, AF8, F1, F2, F3, F4, F5, F6, F7, F8, FC1, FC2, FC3, FC4, FC5, FC6, FT7, FT8, FT9, FT10, C1, C2, C3, C4, C5, C6, T7, T8, CP1, CP2, CP3, CP4, CP5, CP6, TP7, TP8, TP9, TP10, P1, P2, P3, P4, P5, P6, P7, P8, PO3, PO4, PO7, PO8, O1, O2, AFz, Fz, Cz, CPz, Pz, POz and Oz). The reference electrode was placed on FCz and the ground electrode on FPz. Signal impedance was maintained below 5 KΩ. The EEG was recorded with a band-pass filter of 0.01–100 Hz and a slope of 12 dB/oct, amplified by a BrainAmp DC amplifier (Brain Products, Gilching, Germany) and digitized at a sampling rate of 1000 Hz.

For each participant, the EEG data were exported to MATLAB R2021a (MathWorks Inc., Natick MA, USA) and processed offline. The EEG was down-sampled at 500 Hz and filtered with a 1-60 Hz band-pass filter and a 50 Hz notch filter to remove the irrelevant EEG spectral content and the line noise. Stimulus-locked epochs from 0 (stimulus onset) to 6s (stimulus duration), relative to CS onset, were extracted from the continuous EEG. Participant's baseline signal was also extracted from acquisition 1, as the 10 seconds preceding the onset of the first CS, which was used to normalize the data. The baseline and the epochs extracted from all experimental blocks were then concatenated along the time dimension in the following order: baseline, acquisition 1, acquisition 2, reversal 1 and reversal 2. Then, bad channel recognition was performed by computing the correlation coefficient between each electrode and the others. Specifically, for each electrode, the mean value of its 4 highest (absolute) correlations was calculated. Electrodes whose mean value was < 0.4 were marked as bad channels and removed from data (da Cruz et al., 2018). Finally, signals were re-referenced to the average of all electrodes (net of the bad channels) and the online reference electrode (FCz) was recovered.

Following this, an Independent Component Analysis (ICA) was applied to the signals using the infomax algorithm implemented in the Matlab toolbox EEGLAB (https://sccn.ucsd.edu/eeglab/index.php). Then, artefactual components identification and removal *w*as performed using the EEGLAB plugin 'IClabel', that automatically classifies the estimated ICs into seven categories: 'Brain', when originating from cortical patches, or 'Muscle', 'Eye', 'Heart', 'Line Noise', 'Channel Noise' and 'Other', when originating from artifacts or noise. In particular, the classifier reports the probabilities that a given IC belongs to each category. Components labelled as 'Brain' with less than 5% probability were automatically rejected. The remaining components were visually inspected (scalp map, time and spectral activity) and any artefactual component was manually removed. The artifact-cleaned signals were then reconstructed by back-projecting the remaining ICs. Signal concatenation before ICA ensured removal of the same ICs from all experimental blocks and baseline. Finally, bad channels were retrieved using the spherical interpolation method and the 64 EEG signals were re-referenced to the average of all electrodes.

Finally, cortical source activity was reconstructed by estimating intracortical current densities, using the method eLORETA (exact Low Resolution Electromagnetic Tomography, LORETA-KEY©® software package, version: v20200414) (Pascual-Marqui, 1999; Pascual-Marqui et al., 1994). LORETA

uses a three-layers head model (MNI152 template) registered to the Talairach human brain atlas, which provides realistic anatomical information. The solution space is restricted to the grey matter of the reference brain, which is divided in a three-dimensional grid, with a total of 6239 voxels at 5 mm spatial resolution. Each cortical source has its fixed position in a specific point of the grid (voxel) and is characterized by a current density vector with three-dimensional components. In particular, starting from the coordinates of the 64 electrodes, the software LORETA-KEY©® was employed only for the extraction of the inversion matrix of dimension [(3 x 6239) x 64]. Then, for each participant, the three components of the current density of the 6239 voxels were computed in the Matlab environment, by right-multiplying the inversion matrix by the 64 EEG signals. Subsequently, in order to model each dipole as oriented perpendicularly to the cortical surface, the obtained 3D time series of current densities were projected on the voxels' normal versor, obtaining a single time series for each voxel. Then, each voxel was assigned to a specific cortical Region of Interest (ROI) according to the atlas used by LORETA-KEY©® (76 ROIs) and the ROIs' activity was reconstructed by computing the mean activity of the voxels belonging to each ROI. In particular, following the results of previous studies reviewed in the introduction ~~we focused our~~ analyses were focused on ROIs that represented the midcingulate cortex (ROI label: cingulate gyrus), ventral mPFC (ROI label: rectal gyrus), somatosensory cortex (ROI label: postcentral gyrus), motor cortex (ROI label: precentral gyrus) and visual cortex (ROI label: cuneus).

EEG alpha and theta power extraction. Based on previous studies that found that the difference between CS+ and CS- in theta power was maximal during the first 2 seconds of CS presentation (Quirk & Mueller, 2008; Sperl et al., 2019), each epoch was divided into 2-second intervals (i.e. 0-2s, 2-4s, 4-6s), to assess the temporal evolution of changes in power during CS presentation. Then, the Power Spectral Density (PSD) of the ROIs was computed using the Welch's periodogram method (Hamming window of 2 seconds, 50% overlap, 10 seconds zero padding, both for the baseline and 2-second intervals). The power in the theta (4-8 Hz), alpha (8-14 Hz) frequency bands was then calculated for the epochs and baseline. To reduce individual differences between participants and show stimulus-dependent changes in power, for each participant, ~~we normalized~~ the data were normalized by dividing the power of each 2-second interval by that of the baseline. For each participant, this normalized power was then averaged among the 20 CS+ and 20 CS- trials, for each experimental block and used for statistical analysis.

Statistical analyses

Analyses were performed with JASP 0.14.1.0 (JASP Team, 2020) and included frequentist inference. Normality of data distributions was ensured using Q-Q plots, and Shapiro Wilks test (Field, 2013). Repeated-measures analyses of variance (RM ANOVA) were used to investigate differences between more than two conditions followed by planned contrasts, wherever appropriate. Degrees-of-freedom and p-values were Greenhouse–Geisser corrected, whenever a violation of the sphericity assumption occurred. Partial eta-squared (η_p^2) and its 90% confidence interval (CI) were computed as estimates of effect sizes for the ANOVAs' main effects and interactions (Lakens, 2013). In case of significant interactions, interpretation was based on the model estimated marginal means and 95% CI (although means and 95% CI calculated from the raw data are reported in the text and in the plots) (Garofalo et al., 2022). A statistical significance threshold of $p < .05$ was adopted. Note that, in the results, the condition "CS+" refers to the CS+ during acquisition and the new CS+ (old CS-) during reversal, and vice-versa for the condition "CS-".

The dataset used in this manuscript can be found at https://osf.io/nsk65/, and the raw data will be shared by the authors upon request, without undue reservation.

Results

Verbal reports

Two 2 (CS: CS+, CS-) x 4 (phases: Acq1, Acq2, Rev1, Rev2) repeated measures analyses of variance (RM ANOVA) were conducted to test whether and how verbal reports was modulated by CSs association (or absence thereof) with the US, during acquisition and reversal.

Explicit CS-US contingency awareness. ~~We observed~~There was a main effect of CS ($F_{(1, 18)} = 616.12$, $p < .001$, $\eta_p^2 = .97$, 90% CI [0.94, 0.98], indicating higher contingency ratings for the CS+ than CS-, regardless of phase (CS+: M=6.89, SD=0.85; CS-: M=0.46, SD=0.80). No other main effect or interaction was significant (all $p \geq .124$). This analysis confirms the successful acquisition and reversal of contingency awareness in ~~our~~ the experimental group.

Explicit ratings of CSs valence. ~~We observed~~There was a main effect of CS ($F_{(1, 18)} = 45.97$, $p < .001$, $\eta_p^2 = .72$, 90% CI [0.47, 0.81], indicating that the CS+ was judged as less pleasant than CS-, regardless of phase (CS+: M=2.30, SD=1.40; CS-: M=5.97, SD=1.65). No other main effect or interaction was significant (all $p \geq .073$). This analysis confirms the successful acquisition and reversal of valence ratings in the experimental~~our~~ group.

Skin conductance response (SCR)

Due to technical problems, psychophysiological recording for six participants during Rev2 is missing. Thus, the analysis includes only participants whose SCR was recorded in all four phases. Note that performing the same analysis, with all participants but including only the phases before Rev2 did not change the results.

Figure 2A shows the trial-by-trial skin conductance response, averaged across participants. Descriptively, after the first trial of acquisition and reversal, SCR appears greater for the CS+ than the CS-, across almost all remaining trials. A 2 (CS: CS+, CS-) x 4 (phases: Acq1, Acq2, Rev1, Rev2) repeated measures analysis of variance (RM ANOVA) was conducted to test whether and how psychophysiological response was modulated by CSs association (or absence thereof) with the US, during acquisition and reversal. ~~We observed~~There was a main effect of CS ($F_{(1, 12)} = 34.01$, $p < .001$, $\eta_p^2 = .74$, 90% CI [0.42, 0.83], indicating higher SCR for the CS+ than CS-, regardless of phase (CS+: M=0.26, SD=0.19; CS-: M=-0.26, SD=0.19). No other main effect or interaction was significant (all $p \geq .338$). This analysis confirms the successful acquisition and reversal of threat conditioning in the experimental ~~our~~ group.

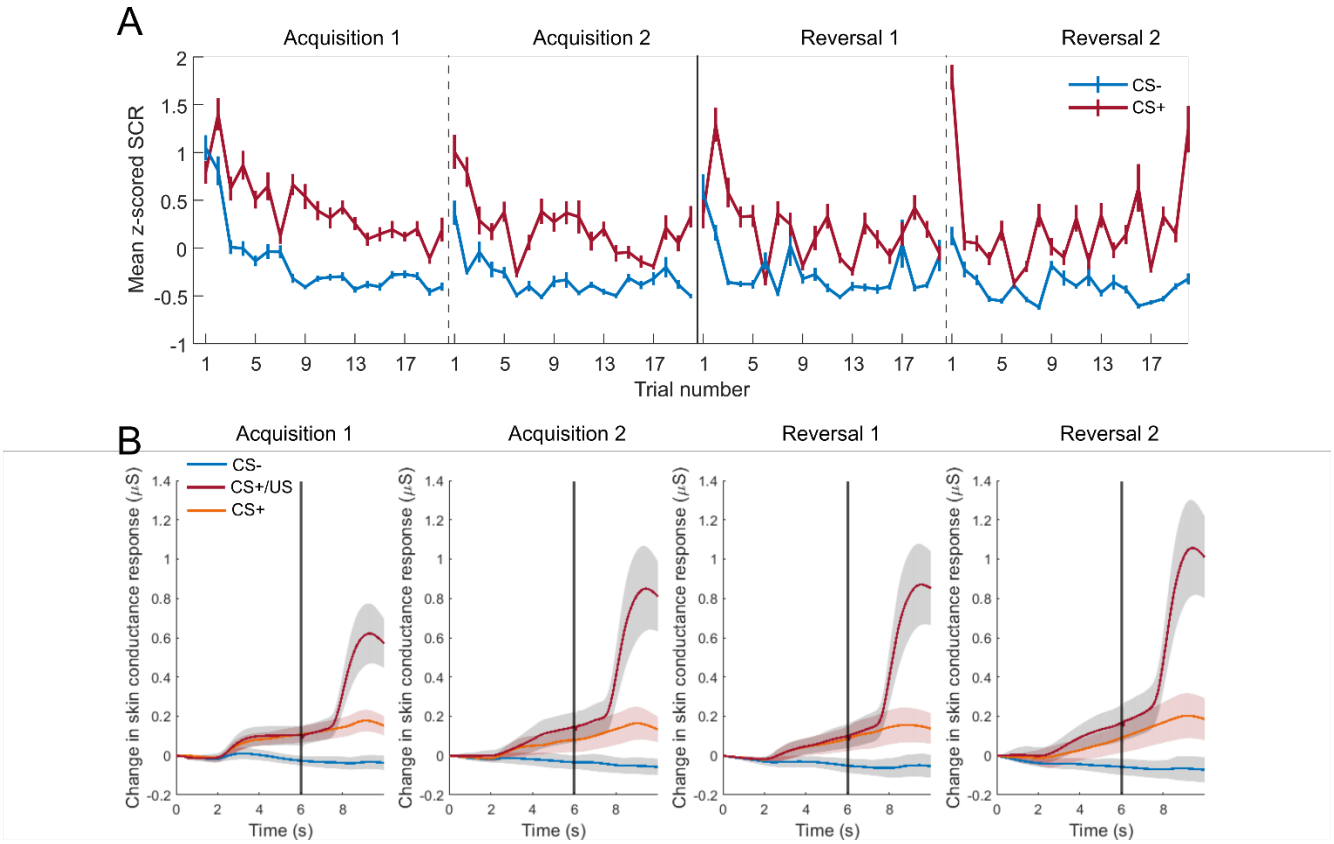

Figure 2. (A) The plot shows trial-by-trial means, and 95% confidence intervals (vertical lines) of z-scored skin conductance response to CS+ and CS-, as a function of the experimental phase (acquisition 1 & 2, or reversal 1 & 2). (B) The figure shows, for each phase, the average change (solid lines), and standard error (shaded area) of skin conductance response during the presentation of the CS-, reinforced CS+ trials (CS+/US) and non-reinforced CS+ trials, as a function of the experimental phase (acquisition 1 & 2, or reversal 1 & 2). The change response is calculated by subtracting the value of the electrodermal response at time 0 seconds. The CS appeared at 0 seconds and disappeared at 6 seconds, when the US was delivered in reinforced trials (represented in the figure by the vertical line).

EEG response

To ensure data quality and enable comparison with other studies, Figure 3 shows differential scalp-level maps (CS+ - CS-) for both theta- and alpha-bands. Normalized theta-band power difference maps show increased activation during CS+ in fronto-medial channels, while normalized alpha-band power difference maps show greater activation during CS- in left parietal channels. The maps at the scalp-level are consistent with those previously ~~results~~ reported in the literature (Babiloni et al., 2003, 2008, 2010, 2014; Bierwirth et al., 2021; Mueller et al., 2014; Sperl et al., 2019) and support the robustness of ~~our~~ the ROI approach on cortical sources, reconstructed from the EEG signals.

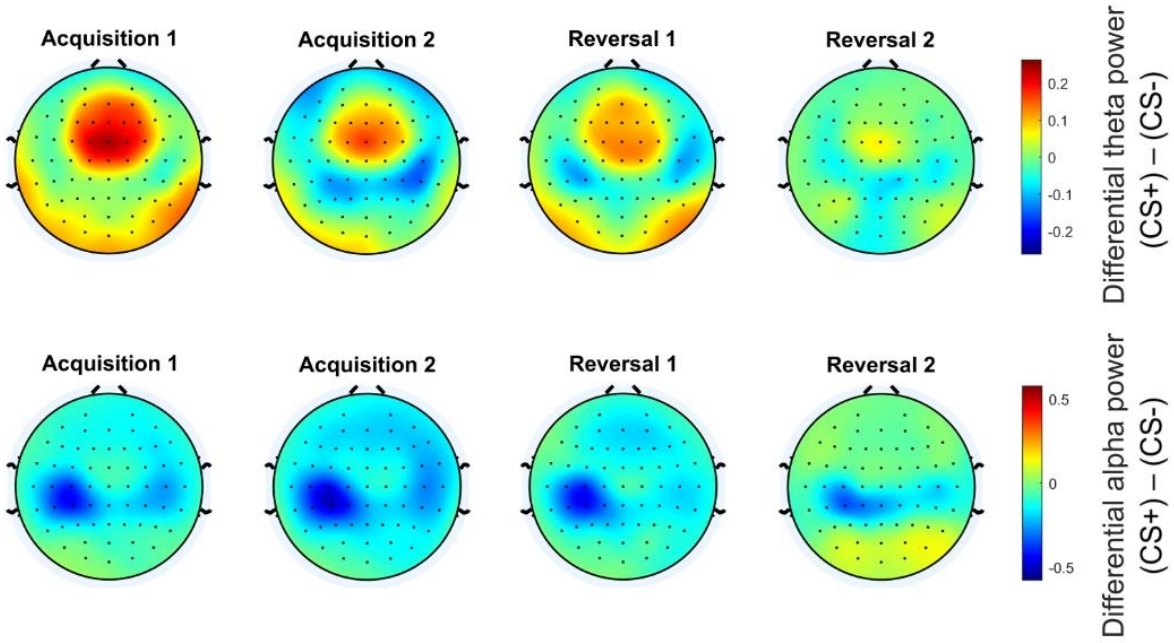

Figure 3. The figure shows the differential (CS+ - CS-) scalp-level maps, for both normalized [top] theta and [bottom] alpha power, as a function of the experimental phase (acquisition 1 & 2, or reversal 1 & 2).

Below, we report the results of the analyses concerning the left hemisphere ROIs. In fact, since the shock was delivered to the right wrist, for the alpha band the analyses focused on the response in contralateral (left) somatosensory and motor ROIs. For the sake of brevity, also the response in the theta band will focus on the left hemisphere ROIs. The results in the same ROIs on the right hemisphere are reported in the supplementary materials.

A series of 2 (type of CS: CS+, CS-) x 4 (phases: Acq1, Acq2, Rev1, Rev2) x 3 (time intervals: 0-2s, 2-4s, 4-6s) repeated measures analyses of variance (RM ANOVAs) was conducted to assess differences in theta and alpha power at the presentation of CS during acquisition and reversal. A sensitivity power analysis (Lakens, 2022) using MorePower 6.0.4 software (Campbell & Thompson, 2012) showed that given ~~our~~ the sample size of 19 participants, $\alpha = .05$ and power=.80, the minimal statistically detectable effect size was: $\eta_p^2 = .33$ for the type of CS (2-level) main effect; $\eta_p^2 = .18$ for the type of CS by phase (2x4) interaction; $\eta_p^2 = .23$ for the type of CS by time interval (2x3) interaction. All these values fall within the 90% CI of the η_p^2 resulting in the analyses below.

Theta. Fig. 4 shows the spatial distribution of the differential normalized theta power (CS+ minus CS-) in the left midcingulate cortex and ventral mPFC. The figure shows a higher theta power in the cingulate cortex during CS+, both during the acquisition and reversal phases. Also, an increase in theta power during CS- is evident in the ventral mPFC during reversal 2. See the statistical analyses below for more details.

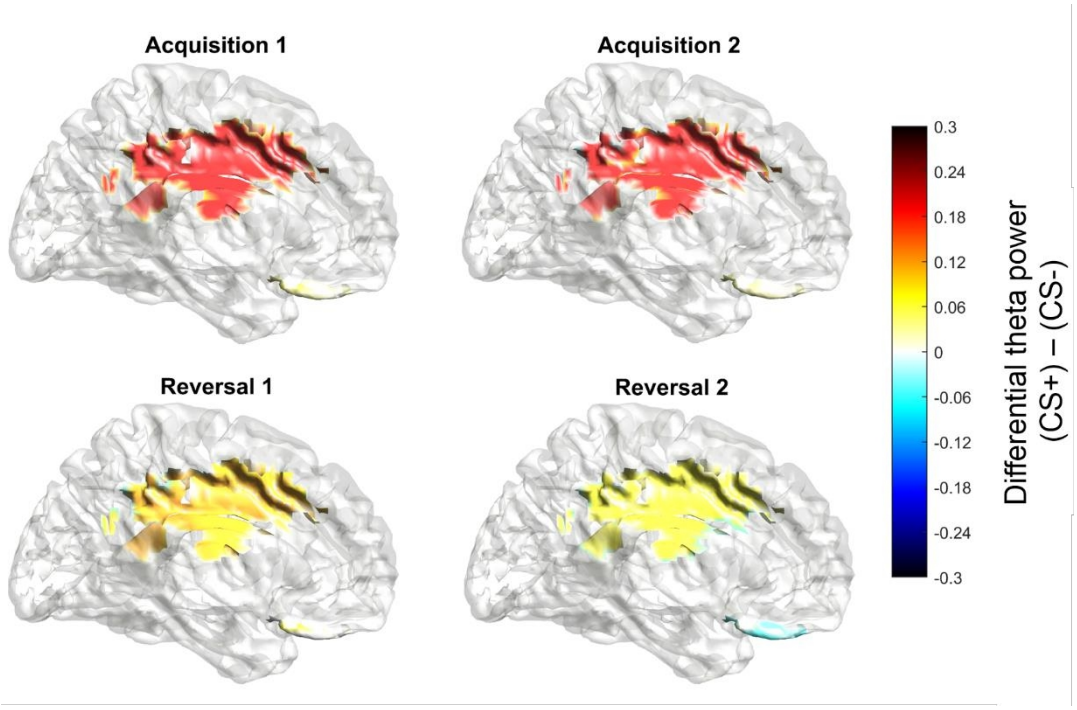

Figure 4. The figure shows the differential normalized theta power (CS+ - CS-) in the midcingulate cortex and ventral mPFC (midsagittal view of left hemisphere) as a function of the experimental phase (acquisition 1 & 2, or reversal 1 & 2).

Midcingulate cortex. The analysis showed a main effect of CS type ($F_{(1, 18)} = 10.49$, $p = .005$, $\eta_p^2 = .37$, 90% CI [0.08, 0.56]), a main effect of time ($F_{(1.40, 25.11)} = 3.93$, $p = .046$, $\eta_p^2 = .18$, 90% CI [0.002, 0.37]), and a CS by time interaction ($F_{(1.28, 23.02)} = 8.91$, $p = .004$, $\eta_p^2 = .33$, 90% CI [0.08, 0.51]). All these effects are clearly evident in figure 5, where the temporal pattern of the normalized theta power is shown for each CS and phase. As it is clear from the figure, the CS by time interaction was explained by a linear increase in power for the CS+ from the first time interval to the following ones. Indeed, theta power was similar between CSs in the 0-2s interval, to then increase over time for the CS+, while remaining stable for the CS- (CS-: $M_{0\text{-}2}$=1.14, $SD_{0\text{-}2}$=0.33, $M_{2\text{-}4}$=1.07, $SD_{2\text{-}4}$ =0.28, $M_{4\text{-}6}$=1.09, $SD_{4\text{-}6}$=0.27; CS+: $M_{0\text{-}2}$=1.13, $SD_{0\text{-}2}$=0.32, $M_{2\text{-}4}$=1.22, $SD_{2\text{-}4}$=0.35, $M_{4\text{-}6}$=1.36, $SD_{4\text{-}6}$=0.46). No other main effect or interaction was significant (all $p \geq .171$; Fig. 5).

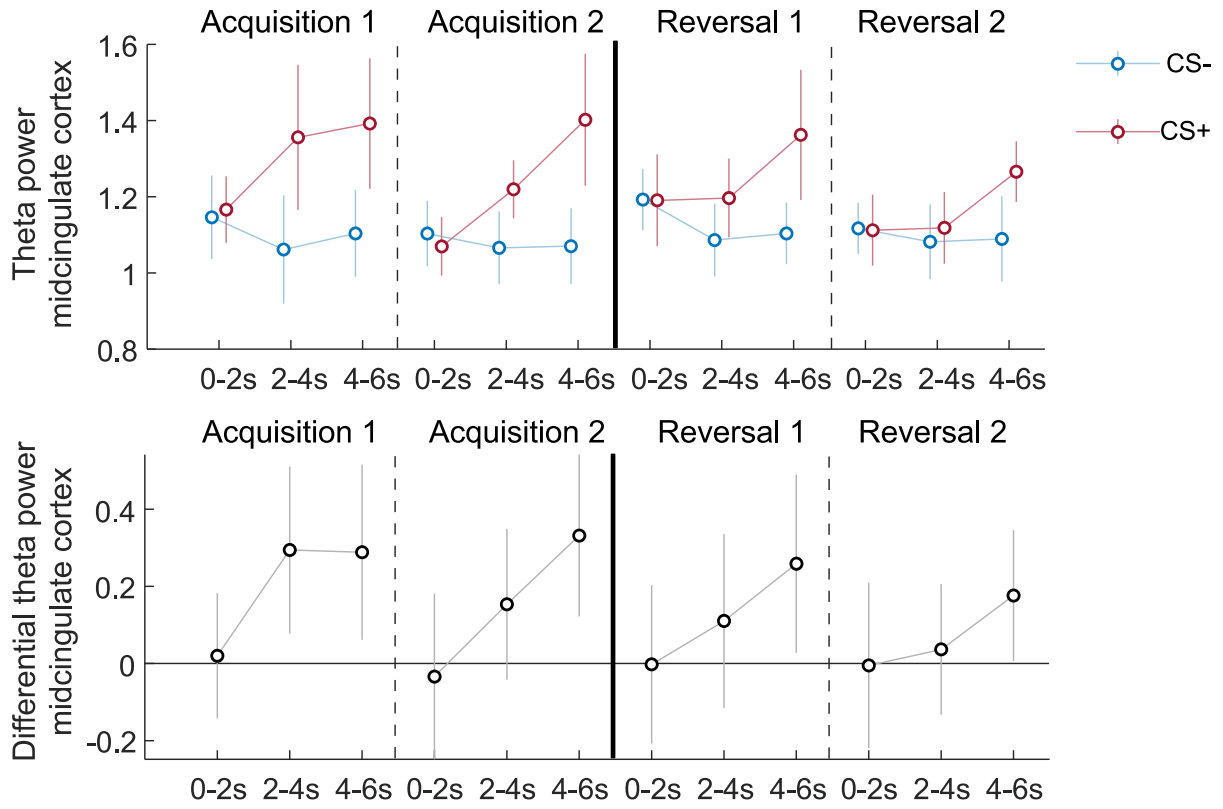

Figure 5. The top plot shows group means (white circles), and 95% confidence intervals (vertical lines) of [top] normalized theta power to CS+ and CS- and [bottom] differential normalized theta power (CS+ - CS-) in the midcingulate cortex, as a function of the experimental phase (acquisition 1 & 2, or reversal 1 & 2) and the time interval (0-2s, 2-4s, 4-6s). 95%CIs were corrected for within-subjects designs (Cousineau, 2005).

Ventral mPFC. The analysis indicated a phase by CS interaction ($F_{(3, 54)} = 3.52$, $p = .021$, $\eta_p^2 = .16$, 90% CI [0.01, 0.28]). Specifically, during acquisition 1 and 2 and reversal 1 theta power appears similar between CS+ and CS- (CS+: M_{acq1}=1.05 SD_{acq1}=0.22, M_{acq2}=1.02, SD_{acq2} =0.23; CS-: M_{acq1}=1.04 SD_{acq1}=0.20, M_{acq2}=0.99, SD_{acq2} =0.23). In contrast, during reversal 2 ~~we observe greater~~ theta power was greater ~~to~~ for the new CS- (old CS+) than the new CS+ (old CS-) (CS+: M_{rev2}=0.95, SD_{rev2}=0.30; CS-: M_{rev2}=1.01, SD_{rev2}=0.33). There was also a CS by time interaction ($F_{(2, 36)} = 3.89$, $p = .030$, $\eta_p^2 = .18$, 90% CI [0.01, 0.33]). Specifically, as shown in figure 6, in the first 2 sec of CS presentation, theta power was greater for the CS- than the CS+ (mainly driven by the reversal phases). In contrast, in the last 2 sec of CS presentation theta power was greater for the CS+ than the CS- (mainly driven by acquisition 2 and reversal 1 phases; CS-: M_{0-2}=1.05 SD_{0-2}=0.30, M_{2-4}=1.00, SD_{2-4} =0.24, M_{4-6}=0.99, SD_{4-6}=0.24; CS+: M_{0-2}=0.99, SD_{0-2}=0.24, M_{2-4} =0.99, SD_{2-4} =0.23, M_{4-6}=1.05, SD_{4-6}=0.30). No other main effect or interaction was significant (all $p \geq .304$).

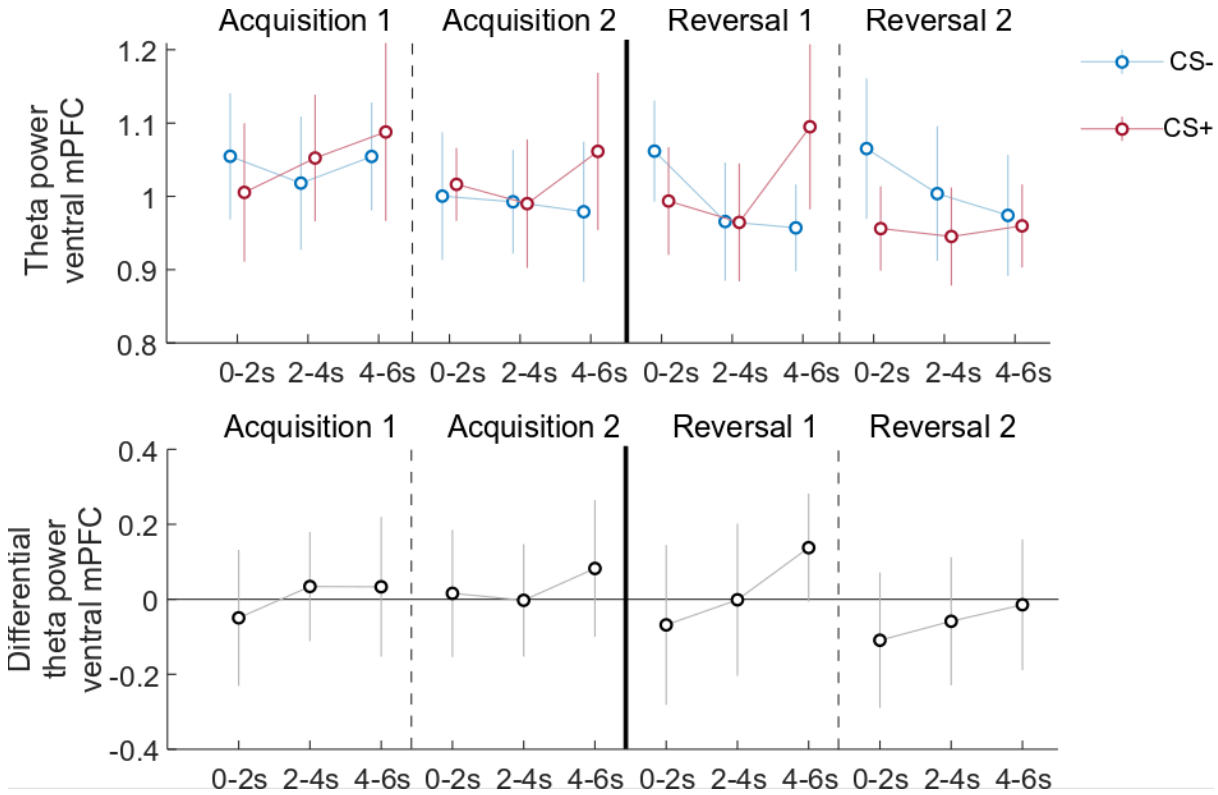

Figure 6. The top plot shows group means (white circles), and 95% confidence intervals (vertical lines) of [top] normalized theta power to CS+ and CS- and [bottom] differential normalized theta power (CS+ - CS-) in the ventral mPFC, as a function of the experimental phase (acquisition 1 & 2, or reversal 1 & 2) and the time interval (0-2s, 2-4s, 4-6s). 95%CIs were corrected for within-subjects designs (Cousineau, 2005).

Alpha. Fig. 7 shows the spatial distribution of the differential normalized alpha power in the left motor, somatosensory and visual cortices. The figure shows an evident decrease in alpha power in the motor cortex during CS+ presentation in all phases, and to a lesser extent in the somatosensory cortex. Additionally, there was a decrease in alpha power during CS+ presentation in the visual cortex during acquisition 2, while there was an increase during reversal 2. See the statistical analyses below for more details.

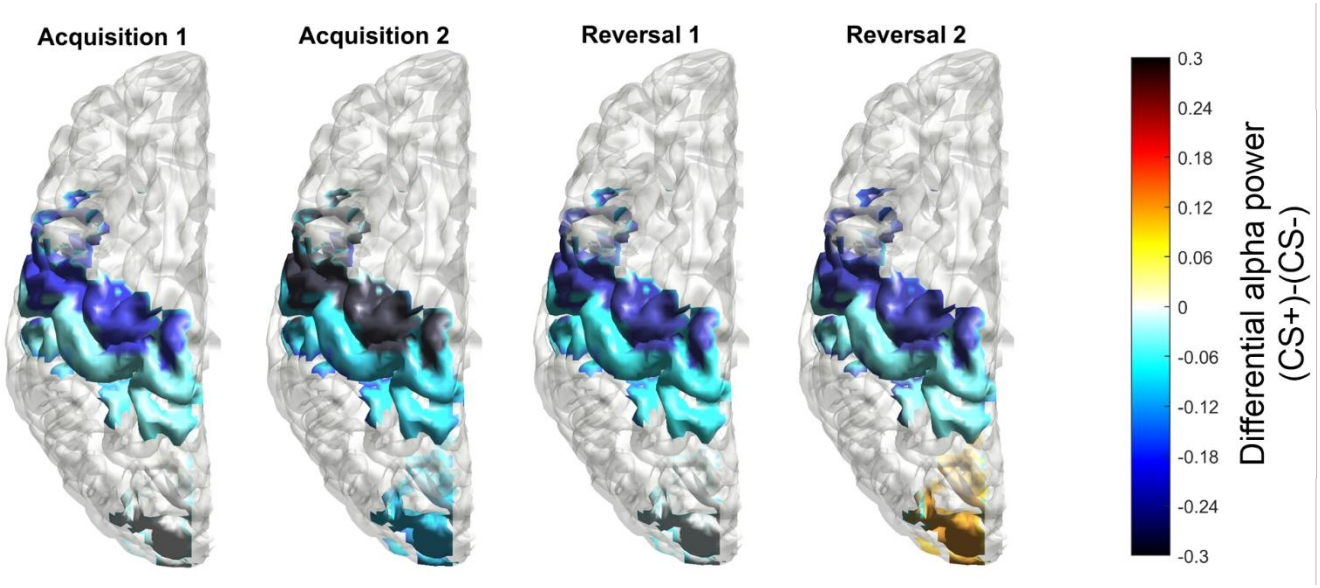

Figure 7. The figure shows the differential normalized alpha power (CS+ - CS-) in the motor cortex, somatosensory cortex and visual cortex (top view of left hemisphere) as a function of the experimental phase (acquisition 1 & 2, or reversal 1 & 2).

Motor cortex. The analysis showed a main effect of CS ($F_{(1,18)} = 6.05$, $p = .024$, $\eta_p^2 = .25$, 90% CI [0.02, 0.47]), indicating greater alpha power for the CS- (M=1.37, SD=0.69) than the CS+ (M=1.10, SD=0.37), regardless of the phase or time window. Such effect is evident in figure 8, which shows the higher normalized power during CS- relative to CS+. No other main effect or interaction was significant (all $p \geq .213$).

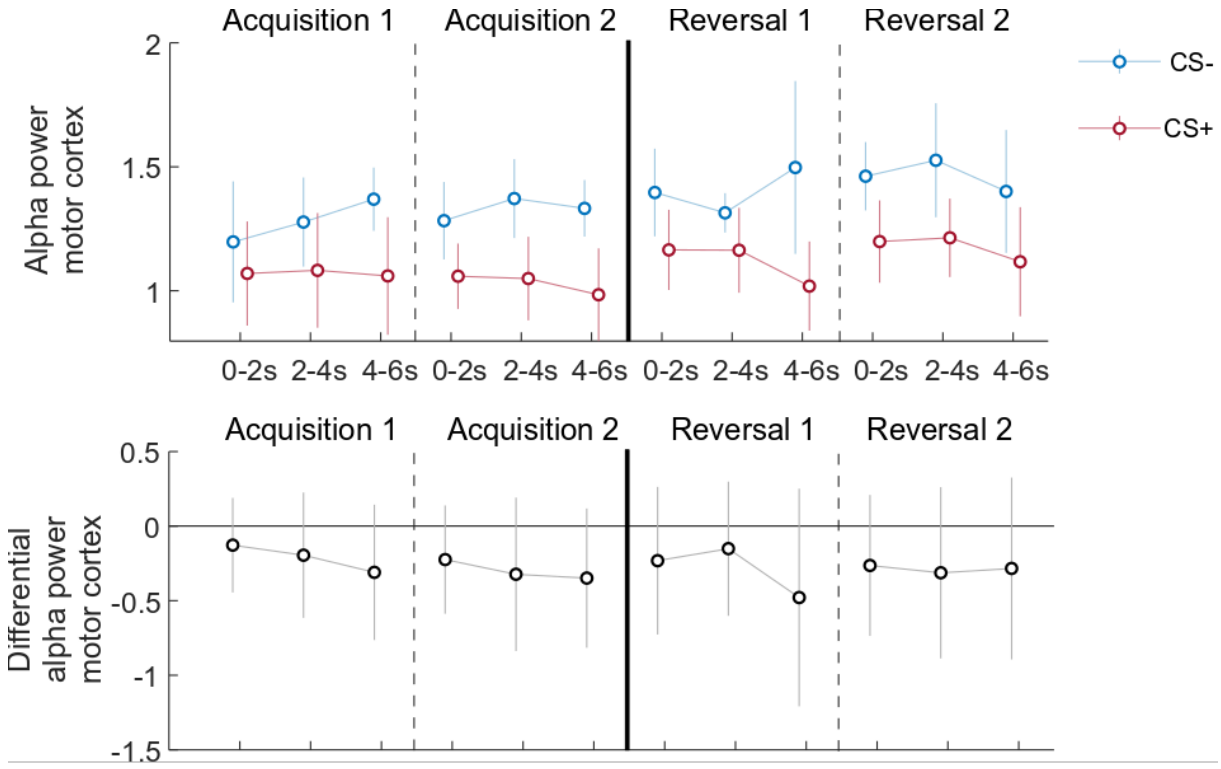

Figure 8. The plot shows group means (white circles), and 95% confidence intervals (vertical lines) of normalized alpha power in the motor cortex to CS+ and CS-, as a function of the experimental phase (acquisition 1 & 2, or reversal 1 & 2) and the time interval (0-2s, 2-4s, 4-6s). 95%CI were corrected for within-subjects designs (Cousineau, 2005).

Somatosensory cortex. The analysis showed a main effect of CS ($F_{(1,18)} = 8.91$, $p = .008$, $\eta_p^2 = .33$, 90% CI [0.06, 0.53]), indicating greater alpha power for the CS- (M=1.07, SD=0.35) than the CS+ (M=1.00, SD=0.35), regardless of the phase or time window, as shown in figure 9. No other main effect or interaction was significant (all p ≥ .232).

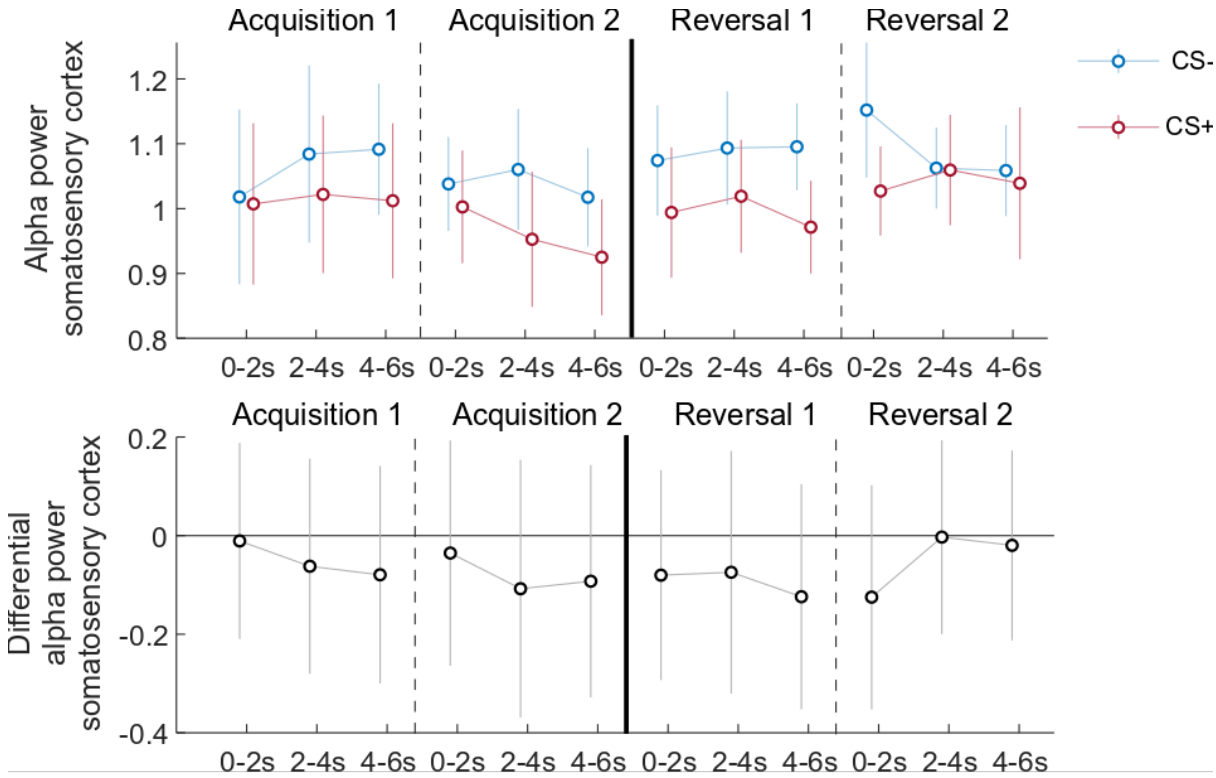

Figure 9. The plot shows group means (white circles), and 95% confidence intervals (vertical lines) of normalized alpha power in the somatosensory cortex to CS+ and CS-, as a function of the experimental phase (acquisition 1 & 2, or reversal 1 & 2) and the time interval (0-2s, 2-4s, 4-6s). 95%CI were corrected for within-subjects designs (Cousineau, 2005).

Visual cortex. The analysis showed a main effect of time ($F_{(2,36)} = 3.52$, $p = .040$, $\eta_p^2 = .16$, 90% CI [0.004, 0.31]), indicating an increase of alpha power from the first 0-2 s to the following 2-4 s and 4-6 s (0-2: *M*=1.03, *SD*=0.45; 2-4: *M*=1.17, *SD*=0.63; 4-6: *M*=1.12, *SD*=0.57), regardless of the CS type or phase. No other main effect or interaction was significant (all p ≥ .240).

Relationship between skin conductance and EEG responses. To assess whether a relationship existed between skin conductance and EEG response, in sources that discriminated between CS+ and CS-, we fitted of a series of linear mixed-effect models on the single-trial data (Spaccasassi et al., 2022), using MATLAB fitlme function. The models included z-scored SCR as the dependent variable, CS type (CS-: CS=0, CS+: CS=1), phase, midcingulate theta power, ventral mPFC theta power, motor cortex alpha power, and somatosensory cortex alpha power as dependent variables. Participants were used as a random effect. Note that for this analysis EEG theta and alpha power were calculated across the entire 6 seconds of CS presentation (Hamming interval of 2 seconds).

Nine different models were tested, and they are reported in detail in Table 1. We tested one model that included only the random effect of participants, four models that included only the main effects of the dependent variables and four models that included also their interaction. Table 1 also reports the Bayesian information criterion (BIC), which provides a quantitative measure of the goodness of fit

associated with each one of the tested models. The model with the lowest BIC was the one including the main effect of the type of CS and of each rhythm, and their interaction, suggesting this as the model that provided the best fit to the SCR data. Thus, we describe the results of this model below.

Table 2 shows the results of the model in detail. The model replicated the effect of CS type on SCR, indicating an increase of SCR when in presence of the CS+, relative to the CS- (b=0.85, 95% CI [0.61, 1.08], $t_{(2790)}$=6.99, p<0.001). Additionally, there was a significant effect of midcingulate theta power, indicating a positive relationship between midcingulate theta power and SCR (b=0.20, 95% CI [0.08, 0.32], $t_{(2790)}$=3.21, p=0.001). ~~We also found~~There was a significant interaction between alpha power from the somatosensory cortex and CS type, indicating a negative relationship between alpha power and SCR for CS+ (b=-0.34, 95% CI [-0.51, -0.18], $t_{(2790)}$=-4.10, p<0.001). Figure 10 shows the relationship between each brain rhythm and SCR for CS+ and CS-.

Table 1. Goodness of fit to z-scored skin conductance responses for individual models using the Bayesian information criterion (BIC; number of observations~~N~~ = 2800)

Formula	BIC
SCR ~ 1 + (1 | id)	7950.8
SCR ~ 1 + theta_midcing + theta_vmPFC + alpha_motor + alpha_somato + (1 | id)	7908.4
SCR ~ 1 + phase + theta_midcing + theta_vmPFC + alpha_motor + alpha_somato + (1 | id)	7913.9
SCR ~ 1 + CS + theta_midcing + theta_vmPFC + alpha_motor + alpha_somato + (1 | id)	7745.1
SCR ~ 1 + phase + CS + theta_midcing + theta_vmPFC + alpha_motor + alpha_somato + (1 | id)	7748
SCR ~ 1 + CS*theta_midcing + CS*theta_vmPFC + CS*alpha_motor + CS*alpha_somato + (1 | id)	**7742.3**
SCR ~ 1 + phase*theta_midcing + phase*theta_vmPFC + phase*alpha_motor + phase*alpha_somato + (1 | id)	7992.5
SCR ~ 1 + phase*theta_midcing + CS*theta_mid.cing + phase*theta_vmPFC + CS*theta_vmPFC… + phase*alpha_motor + CS*alpha_motor + phase*alpha_somato + CS*alpha_somato + (1 | id)	7825.1
SCR ~ 1 + theta_midcing*CS*phase + theta_vmPFC*CS*phase + alpha_motor*CS*phase... + alpha_somato*CS*phase + (1|id)	7928.5

Note. SCR= z-scored skin conductance response; theta_midcing = normalized theta power from the midcingulate cortex; theta_vmPFC= normalized theta power from the ventral mPFC; alpha_motor = normalized alpha power from the motor cortex; alpha_somato = normalized alpha power from the somatosensory cortex; id=participant number. The model in bold is the one with the lowest BIC.

Table 2. Coefficient estimate for each model term, with their standard error, their lower and upper limit of the 95% confidence interval (CI), t-statistic for each coefficient, degrees of freedom and p-value.

Name	Estimate (b)	Standar d Error	Lower CI	Upper CI	t	df	p
Intercept	-0.43	0.09	-0.60	-0.27	-5.09	2790	0.000*
CS (CS+: CS=1, CS-: CS=0)	0.85	0.12	0.61	1.08	6.99	2790	0.000*
Theta_midcing	0.20	0.06	0.08	0.32	3.21	2790	0.001*
Theta_vmPFC	-0.05	0.07	-0.18	0.08	-0.76	2790	0.447
Alpha_motor	-0.04	0.03	-0.09	0.01	-1.51	2790	0.130
Alpha_somato	0.05	0.05	-0.05	0.16	1.02	2790	0.310
CS*theta_midcing	-0.06	0.08	-0.22	0.09	-0.83	2790	0.409
CS*theta_vmPFC	0.15	0.10	-0.04	0.33	1.52	2790	0.128
CS*alpha_motor	-0.07	0.06	-0.18	0.04	-1.21	2790	0.226
CS*alpha_somato	-0.34	0.08	-0.51	-0.18	-4.10	2790	0.000*

Note. theta_midcing = normalized theta power from the midcingulate cortex; theta_vmPFC= normalized theta power from the ventral mPFC; alpha_motor = normalized alpha power from the motor cortex; alpha_somato = normalized alpha power from the somatosensory cortex. * indicates significant effects. The linear model equation associated with this model is SCR = -0.43+0.85*cs+0.20*theta_midcing-0.05*theta_vmPFC-0.04*alpha_motor+0.05*alpha_somato-0.06*CS*theta_midcing +0.15*CS*theta_vmPFC -0.07*CS*alpha_motor-0.34*CS*alpha_somato

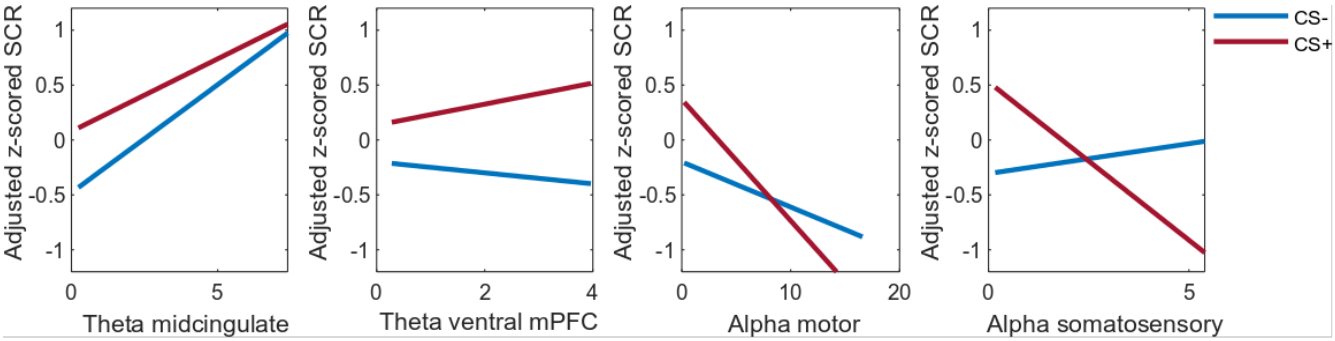

Figure 10. Interaction plots that show the adjusted z-score SCR as a function of each brain rhythm for CS- and CS+. The results of the linear mixed model analysis indicated a significant positive relationship between midcingulate theta power and SCR, and a significant negative relationship between somatosensory alpha power and SCR for CS+. The plots were produced using the MATLAB function "plotInteraction". The function plots the adjusted response function (adjusted z-score SCR) as a function of one predictor (brain rhythm), with the other predictor (CS type) fixed at specific values. The adjusted response function describes the relationship between the fitted response and a single predictor, with the other predictors averaged out by averaging the fitted values over the data used in the fit.

Discussion

We tested whether changes in theta and alpha brain oscillations marked the acquisition and reversal of threat predictions and correlated with skin conductance response (SCR), a peripheral marker of threat learning. To this end, electroencephalogram and electrodermal activity were recorded in a group of healthy adults, who completed a Pavlovian threat conditioning task that included an acquisition and a reversal phase. During acquisition, presentation of a visual stimulus, was paired with delivery of an aversive shock (CS+), while another visual stimulus, served as within-subject control condition (CS-) and was never paired with the shock. During reversal, the picture-shock contingencies were switched, such that the old CS+ was now the new CS- and the old CS- was the new CS+. ~~We found~~Results showed that the power of both theta and alpha discriminated between threat and safety, showing a differential response between CS+ and CS-, but with unique modulations for each rhythm, localized in specific cortical sources and as a function of the experimental phase (acquisition or reversal). Additionally, a relationship was found between single trial theta and alpha power and skin conductance response, establishing a direct relationship between activation of the central and peripheral nervous systems during learning.

~~We initially confirmed~~First, the acquisition and reversal of threat predictions in participants was confirmed from SCR and subjective reports of stimulus valence and stimulus-outcome contingency; the CS+ elicited greater SCR, and was judged as less pleasant and more contingent with US delivery than the CS-. Such responses were observed regardless of the experimental phase. Thus, as the identity of the shock-paired picture was switched from acquisition to reversal (i.e. acquisition: picture A = CS+, picture B = CS-; reversal: picture B = new CS+/old CS-, picture A = new CS-/old CS+), so did the SCR, subjective pleasantness and explicit CS-US contingency.

Concerning brain rhythms, theta oscillations showed a complex dynamic over the course of the task, varying their power to CSs depending on the examined source. Specifically, midcingulate cortex theta power was greater for the CS+ than the CS-, regardless of the phase. Thus, similarly to SCR and subjective reports, midcingulate cortex theta power tracked the motivational value of the stimuli, as they acquired or reversed their threat-related value, showing a corresponding change in power that discriminated between CS+ and CS-. Crucially, ~~we also found that~~ theta power in the midcingulate cortex changed over the 6 seconds of CS presentation, showing a linear increase in power for the CS+ as timed approached shock delivery, while remaining stable during CS- presentation. This ramp-like increase of theta for the shock-paired CS+ suggests the possibility of a temporal encoding of US arrival by theta. Indeed, timing of outcome occurrence is a core part of associative learning (Kirkpatrick & Balsam, 2016; Nasser & Delamater, 2016). For example, timing of conditioned responses, such as eyelid closure, is often tuned to the expected time of US presentation (Kirkpatrick & Balsam, 2016; Nasser & Delamater, 2016; Sutton & Barto, 1998), while unexpected timing of aversive US delivery has been shown to evoke a prediction error signal (Garofalo et al., 2014, 2017; Magosso et al., 2015). Thus, midcingulate theta may be another contributor to such temporal learning, in line with the idea of a general role of the cingulate cortex in event prediction (Alexander & Brown, 2011), even when outcomes are not contingent to actions (Alexander & Brown, 2014). Whether this ramp-like theta response continues even after CS+ disappearance, in particular when no US is delivered, may warrant further investigation, to clarify the putative role of theta in temporal learning. Note that this temporal dynamic of theta is in contrast with previous studies, which found greater mediofrontal theta power to the CS+ than the CS- limited to the first 2 seconds of CS presentation (Bierwirth et al., 2021; Mueller et al., 2014; Sperl et al., 2019). Importantly, such studies tested the recall of previously acquired threat predictions, rather than the initial learning of predictions, and used a shorter CS presentation, of 4

rather than 6 seconds. Thus, whether such differences in results depend on the process investigated – acquisition and reversal, or subsequent recall – or on the duration of stimuli warrants further research. Nevertheless, the overall greater midcingulate theta for the CS+ extends the previous literature on the theta rhythm (Bierwirth et al., 2021; Mueller et al., 2014; Sperl et al., 2019), showing its role in threat learning during acquisition and reversal.

In the ventral mPFC, theta power showed a unique modulation as a function of the experimental phase. While during acquisition 1 and 2 and reversal 1 theta power appears similar between CS+ and CS-, during reversal 2, theta power became greater to the new CS- (old CS+) than the new CS+ (old CS-). In line with the neuroimaging literature that shows a role of the ventral mPFC during reversal (Savage et al., 2020; Schiller et al., 2008; Zhang et al., 2015), increased theta power to the new CS- (old CS+) as compared to the new CS+ (old CS-) in reversal is compatible with the inhibition of a previously learned threat response that is no longer appropriate, due to CSs-US contingencies reversal. Taken together, the results on theta power provide evidence for a functional heterogeneity of this rhythm along midline cortical regions during the acquisition and reversal of threat predictions. While theta power in the midcingulate cortex tracks the stimulus current motivational value, timely preparing the organism to respond to the upcoming danger, in the ventral mPFC, theta power may reflect a response inhibition process. Such heterogeneity appears in line with the previous literature that has linked increases in theta power to the encoding of fear, safety and/or cognitive control (Bierwirth et al., 2021; Cavanagh et al., 2012, 2013; Mueller et al., 2014; Sangha et al., 2020; Sperl et al., 2019).

Alpha power also appeared to play a role in threat learning, showing its unique modulation in response to the two CSs. Specifically, ~~we found lower~~ alpha power was lower for the CS+ than the CS- from the precentral and postcentral gyri, regardless of the phase. Thus, similarly to SCR and midcingulate cortex theta power, alpha power tracked the motivational value of the stimuli, as they acquired or reversed their threat-related value. The alpha desynchronization for the CS+ mimics findings of greater alpha desynchronization at somato-motor electrode sites in anticipation of painful somatosensory stimuli (Babiloni et al., 2003, 2008, 2010, 2014). This somato-motor alpha change is suggestive of cross-modal conditioning-induced plasticity, with the visual CS+ eliciting a conditioned response of the somatosensory cortex matching the US modality, rather than the CS+ modality (Miskovic & Keil, 2012). Additionally, this effect was not found in the cuneus, indicating no evidence of unimodal conditioning-induced plasticity (but see Panitz et al., 2019; Yin et al., 2020). Overall, the decreased alpha power for the CS+ from the motor and somatosensory cortices may reflect enhanced activation of the somato-motor system, in preparation of the aversive outcome. Unlike the theta rhythm, the difference in alpha power between CSs did not show any temporal evolution over the 6 seconds of CS presentation. This possibly suggests a rapid discrimination of the two CSs by the somato-motor system that is maintained during the entire presentation of the CS.

Finally, the results of the linear mixed effect models on single trial data showed a positive relationship between midcingulate theta power and skin conductance response, regardless of the stimulus, and a negative relationship between somatosensory alpha power and skin conductance response for the CS+. Thus, while an increase in midcingulate theta was related to a general increase in skin conductance response, a decrease in somatosensory alpha was related to an increase in skin conductance in response to the CS+. Such results may suggest a direct relationship between response of the central and peripheral nervous systems during threat learning, with both the alpha and theta rhythms being correlated with the peripheral expression of threat learning, possibly to ensure the timely preparation of responses to the upcoming danger. Indeed, an increase in skin conductance has been reported immediately before the initiation of responses in an active avoidance task (Löw et al., 2015), and more

broadly, activation of the sympathetic nervous system facilitates action and is characteristic of active defense behaviors (Cannon, 1939; Critchley, 2002; Hamm, 2020; Starita et al., 2022).

Overall, both alpha and theta appear to contribute to the initial acquisition and reversal of threat predictions, flexibly regulating the expression of threat responses in the face of changing stimulus-outcome contingencies. The unique modulations of theta and alpha power to each CS, across acquisition and reversal, highlight the existence of multiple systems that contribute to the expression of threat learning. Possibly, while changes in theta in the midcingulate cortex may have a crucial role in learning the timing of the upcoming danger, alpha power may reflect the preparation of the somato-motor system to the upcoming danger. Additionally, in the ventral medial prefrontal cortex the theta rhythm may play an inhibitory role of responses that are no longer appropriate. Together, the observed changes in theta and alpha may be crucial for the successful enactment of defensive responses and survival in an ever-changing environment. Further validation of this functional interpretation of brain rhythms may be achieved using mechanistic neural network models of oscillating brain populations (Ursino et al., 2010), reciprocally interconnected according to a biologically inspired connectivity. Indeed, such models have been recently used to analyze essential phenomena, such as the genesis of brain rhythms during sleep (Cona et al., 2014), the function of theta-gamma coupling in the hippocampus (Cona & Ursino, 2013, 2015), the role of rhythms in working memory (Ursino et al., 2022). Hence, they represent a valid instrument to test the present interpretation on the role of each rhythm in the acquisition and reversal of threat predictions.

References

Alexander, W. H., & Brown, J. W. (2011). Medial prefrontal cortex as an action-outcome predictor. *Nature Neuroscience*, *14*(10), 1338–1344. https://doi.org/10.1038/nn.2921

Alexander, W. H., & Brown, J. W. (2014). A general role for medial prefrontal cortex in event prediction. *Frontiers in Computational Neuroscience*, *8*(July), 1–11. https://doi.org/10.3389/fncom.2014.00069

Arnal, L. H., & Giraud, A.-L. (2012). Cortical oscillations and sensory predictions. *Trends in Cognitive Sciences*, *16*, 390–398. https://doi.org/10.1016/j.tics.2012.05.003

Babiloni, C., Brancucci, A., Babiloni, F., Capotosto, P., Carducci, F., Cincotti, F., Arendt-Nielsen, L., Chen, A. C. N., & Rossini, P. M. (2003). Anticipatory cortical responses during the expectancy of a predictable painful stimulation. A high-resolution electroencephalography study. *European Journal of Neuroscience*, *18*(6), 1692–1700. https://doi.org/10.1046/j.1460-9568.2003.02851.x

Babiloni, C., Capotosto, P., Brancucci, A., Del Percio, C., Petrini, L., Buttiglione, M., Cibelli, G., Romani, G. L., Rossini, P. M., & Arendt-Nielsen, L. (2008). Cortical Alpha Rhythms Are Related to the Anticipation of Sensorimotor Interaction Between Painful Stimuli and Movements: A High-Resolution EEG Study. *Journal of Pain*, *9*(10), 902–911. https://doi.org/10.1016/j.jpain.2008.05.007

Babiloni, C., Capotosto, P., Del Percio, C., Babiloni, F., Petrini, L., Buttiglione, M., Cibelli, G., Marusiak, J., Romani, G. L., Arendt-Nielsen, L., & Rossini, P. M. (2010). Sensorimotor interaction between somatosensory painful stimuli and motor sequences affects both anticipatory alpha rhythms and behavior as a function of the event side. *Brain Research Bulletin*, *81*(4–5), 398–405. https://doi.org/10.1016/j.brainresbull.2009.11.009

Babiloni, C., Percio, C. Del, Arendt-Nielsen, L., Soricelli, A., Romani, G. L., Rossini, P. M., & Capotosto, P. (2014). Cortical EEG alpha rhythms reflect task-specific somatosensory and motor interactions in humans. *Clinical Neurophysiology*, *125*, 1936–1945. https://doi.org/10.1016/j.clinph.2014.04.021

Bach, D. R., Daunizeau, J., Friston, K. J., & Dolan, R. J. (2010). Dynamic causal modelling of anticipatory skin conductance responses. *Biological Psychology*, *85*(1), 163–170. https://doi.org/10.1016/j.biopsycho.2010.06.007

Barry, R. J., Clarke, A. R., Johnstone, S. J., Magee, C. A., & Rushby, J. A. (2007). EEG differences between eyes-closed and eyes-open resting conditions. *Clinical Neurophysiology*, *118*(12), 2765–2773. https://doi.org/10.1016/j.clinph.2007.07.028

Battaglia, S., Garofalo, S., di Pellegrino, G., & Starita, F. (2020). Revaluing the Role of vmPFC in the Acquisition of Pavlovian Threat Conditioning in Humans. *The Journal of Neuroscience*, *40*(44), 8491–8500. https://doi.org/10.1523/JNEUROSCI.0304-20.2020

Beckers, T., Krypotos, A. M., Boddez, Y., Effting, M., & Kindt, M. (2013). What's wrong with fear conditioning? *Biological Psychology*, *92*(1), 90–96. https://doi.org/10.1016/j.biopsycho.2011.12.015

Bierwirth, P., Sperl, M. F. J., Antov, M. I., & Stockhorst, U. (2021). Prefrontal Theta Oscillations Are Modulated by Estradiol Status During Fear Recall and Extinction Recall. *Biological Psychiatry:*

Cognitive Neuroscience and Neuroimaging, *6*(11), 1071–1080. https://doi.org/10.1016/j.bpsc.2021.02.011

Boucsein, W., Fowles, D. C., Grimnes, S., Ben-Shakhar, G., Roth, W. T., Dawson, M. E., & Filion, D. L. (2012). Publication recommendations for electrodermal measurements. *Psychophysiology*, *49*(8), 1017–1034. https://doi.org/10.1111/J.1469-8986.2012.01384.X

Campbell, J. I. D. D., & Thompson, V. A. (2012). MorePower 6.0 for ANOVA with relational confidence intervals and Bayesian analysis. *Behavior Research Methods*, *44*(4), 1255–1265. https://doi.org/10.3758/s13428-012-0186-0

Cannon, W. B. (1939). *The wisdom of the body* (Norton & Co. (ed.); 2nd ed.).

Cavanagh, J. F., Eisenberg, I., Guitart-Masip, M., Huys, Q., & Frank, M. J. (2013). Frontal Theta Overrides Pavlovian Learning Biases. *Journal of Neuroscience*, *33*(19), 8541–8548. https://doi.org/10.1523/JNEUROSCI.5754-12.2013

Cavanagh, J. F., & Frank, M. J. (2014). Frontal theta as a mechanism for cognitive control. *Trends in Cognitive Sciences*, *18*(8), 414–421. https://doi.org/10.1016/j.tics.2014.04.012

Cavanagh, J. F., Frank, M. J., Klein, T. J., & Allen, J. J. B. (2010). Frontal theta links prediction errors to behavioral adaptation in reinforcement learning. *NeuroImage*, *49*(4), 3198–3209. https://doi.org/10.1016/j.neuroimage.2009.11.080

Cavanagh, J. F., Zambrano-Vazquez, L., & Allen, J. J. B. (2012). Theta lingua franca: A common mid-frontal substrate for action monitoring processes. *Psychophysiology*, *49*(2), 220–238. https://doi.org/10.1111/j.1469-8986.2011.01293.x

Chen, S., Tan, Z., Xia, W., Gomes, C. A., Zhang, X., Zhou, W., Liang, S., Axmacher, N., & Wang, L. (2021). Theta oscillations synchronize human medial prefrontal cortex and amygdala during fear learning. *Science Advances*, *7*(34), 4198–4216. https://doi.org/10.1126/SCIADV.ABF4198/SUPPL_FILE/SCIADV.ABF4198_SM.PDF

Cona, F., Lacanna, M., & Ursino, M. (2014). A thalamo-cortical neural mass model for the simulation of brain rhythms during sleep. *Journal of Computational Neuroscience*, *37*(1), 125–148. https://doi.org/10.1007/s10827-013-0493-1

Cona, F., & Ursino, M. (2013). A MULTI-LAYER NEURAL-MASS MODEL FOR LEARNING SEQUENCES USING THETA/GAMMA OSCILLATIONS. *International Journal of Neural Systems*, *23*(03), 1250036. https://doi.org/10.1142/S0129065712500360

Cona, F., & Ursino, M. (2015). A neural mass model of place cell activity: theta phase precession, replay and imagination of never experienced paths. *Journal of Computational Neuroscience*, *38*(1), 105–127. https://doi.org/10.1007/S10827-014-0533-5/TABLES/4

Cousineau, D. (2005). Confidence intervals in within-subject designs: A simpler solution to Loftus and Masson's method. *Tutorials in Quantitative Methods for Psychology*, *1*(1), 42–45. https://doi.org/10.20982/tqmp.01.1.p042

Critchley, H. D. (2002). Review: Electrodermal Responses: What Happens in the Brain. *The Neuroscientist*, *8*(2), 132–142. https://doi.org/10.1177/107385840200800209

da Cruz, J. R., Chicherov, V., Herzog, M. H., & Figueiredo, P. (2018). An automatic pre-processing

pipeline for EEG analysis (APP) based on robust statistics. *Clinical Neurophysiology*, *129*(7), 1427–1437. https://doi.org/10.1016/J.CLINPH.2018.04.600

Duits, P., Cath, D. C., Lissek, S., Hox, J. J., Hamm, A. O., Engelhard, I. M., Van Den Hout, M. A., & Baas, J. M. P. (2015). Updated meta-analysis of classical fear conditioning in the anxiety disorders. *Depression and Anxiety*, *32*(4), 239–253. https://doi.org/10.1002/da.22353

Effting, M., & Kindt, M. (2007). Contextual control of human fear associations in a renewal paradigm. *Behaviour Research and Therapy*, *45*(9), 2002–2018. https://doi.org/10.1016/J.BRAT.2007.02.011

Field, A. (2013). Discovering statistics using IBM SPSS statistics. In *Statistics*.

Fullana, M. A., Albajes-Eizagirre, A., Soriano-Mas, C., Vervliet, B., Cardoner, N., Benet, O., Radua, J., & Harrison, B. J. (2018). Fear extinction in the human brain: A meta-analysis of fMRI studies in healthy participants. *Neuroscience & Biobehavioral Reviews*, *88*, 16–25. https://doi.org/10.1016/J.NEUBIOREV.2018.03.002

Fullana, M. A., Harrison, B. J., Soriano-Mas, C., Vervliet, B., Cardoner, N., Àvila-Parcet, A., & Radua, J. (2016). Neural signatures of human fear conditioning: an updated and extended meta-analysis of fMRI studies. *Molecular Psychiatry*, *21*(4), 500–508. https://doi.org/10.1038/mp.2015.88

Garofalo, S., Giovagnoli, S., Orsoni, M., Starita, F., & Benassi, M. (2022). Interaction effect: Are you doing the right thing? *PLOS ONE*, *17*(7), e0271668. https://doi.org/10.1371/journal.pone.0271668

Garofalo, S., Maier, M. E., & di Pellegrino, G. (2014). Mediofrontal negativity signals unexpected omission of aversive events. *Scientific Reports*, *4*(1), 1–7. https://doi.org/10.1038/srep04816

Garofalo, S., Sagliano, L., Starita, F., Trojano, L., & di Pellegrino, G. (2020). Subliminal determinants of cue-guided choice. *Scientific Reports*, *10*(1), 11926. https://doi.org/10.1038/s41598-020-68926-y

Garofalo, S., Timmermann, C., Battaglia, S., Maier, M. E., & di Pellegrino, G. (2017). Mediofrontal Negativity Signals Unexpected Timing of Salient Outcomes. *Journal of Cognitive Neuroscience*, *29*(4), 718–727. https://doi.org/10.1162/jocn_a_01074

Green, S. R., Kragel, P. A., Fecteau, M. E., & LaBar, K. S. (2014). Development and validation of an unsupervised scoring system (Autonomate) for skin conductance response analysis. *International Journal of Psychophysiology*, *91*(3), 186–193. https://doi.org/10.1016/j.ijpsycho.2013.10.015

Hajihosseini, A., & Holroyd, C. B. (2013). Frontal midline theta and N200 amplitude reflect complementary information about expectancy and outcome evaluation. *Psychophysiology*, *50*(6), 550–562. https://doi.org/10.1111/psyp.12040

Hamm, A. O. (2020). Fear, anxiety, and their disorders from the perspective of psychophysiology. *Psychophysiology*, *57*(2), e13474. https://doi.org/10.1111/PSYP.13474

Kirkpatrick, K., & Balsam, P. D. (2016). Associative learning and timing. *Current Opinion in Behavioral Sciences*, *8*, 181–185. https://doi.org/10.1016/j.cobeha.2016.02.023

Krypotos, A.-M., Arnaudova, I., Effting, M., Kindt, M., & Beckers, T. (2015). Effects of Approach-Avoidance Training on the Extinction and Return of Fear Responses. *PLOS ONE*, *10*(7), e0131581. https://doi.org/10.1371/journal.pone.0131581

Krypotos, A.-M., Effting, M., Arnaudova, I., Kindt, M., & Beckers, T. (2014). Avoided by association: Acquisition, extinction, and renewal of avoidance tendencies toward conditioned fear stimuli. *Clinical Psychological Science*, *2*(3), 336–343. https://doi.org/10.1177/2167702613503139

Lakens, D. (2013). Calculating and reporting effect sizes to facilitate cumulative science: a practical primer for t-tests and ANOVAs. *Frontiers in Psychology*, *4*(1). https://doi.org/10.3389/fpsyg.2013.00863

Lakens, D. (2022). Sample Size Justification. *Collabra: Psychology*, *8*(1), 1–31. https://doi.org/10.1525/collabra.33267

Lonsdorf, T. B., Klingelhöfer-Jens, M., Andreatta, M., Beckers, T., Chalkia, A., Gerlicher, A., Jentsch, V. L., Drexler, S. M., Mertens, G., Richter, J., Sjouwerman, R., Wendt, J., & Merz, C. J. (2019). Navigating the garden of forking paths for data exclusions in fear conditioning research. *ELife*, *8*. https://doi.org/10.7554/eLife.52465

Lonsdorf, T. B., Menz, M. M., Andreatta, M., Fullana, M. A., Golkar, A., Haaker, J., Heitland, I., Hermann, A., Kuhn, M., Kruse, O., Meir Drexler, S., Meulders, A., Nees, F., Pittig, A., Richter, J., Römer, S., Shiban, Y., Schmitz, A., Straube, B., … Merz, C. J. (2017). Don't fear 'fear conditioning': Methodological considerations for the design and analysis of studies on human fear acquisition, extinction, and return of fear. *Neuroscience & Biobehavioral Reviews*, *77*, 247–285. https://doi.org/10.1016/j.neubiorev.2017.02.026

Löw, A., Weymar, M., & Hamm, A. O. (2015). When Threat Is Near, Get Out of Here: Dynamics of Defensive Behavior During Freezing and Active Avoidance. *Psychological Science*, *26*(11), 1706–1716. https://doi.org/10.1177/0956797615597332

Lykken, D. T., & Venables, P. H. (1971). DIRECT MEASUREMENT OF SKIN CONDUCTANCE: A PROPOSAL FOR STANDARDIZATION. *Psychophysiology*, *8*(5), 656–672. https://doi.org/10.1111/j.1469-8986.1971.tb00501.x

Magosso, E., Forcelli, V., Garofalo, S., Di Pellegrino, G., & Ursino, M. (2015). Event-related brain potential signaling unexpected timing of feedback: A source localization analysis. *Proceedings of the Annual International Conference of the IEEE Engineering in Medicine and Biology Society, EMBS*, *2015-November*, 618–621. https://doi.org/10.1109/EMBC.2015.7318438

Mathôt, S., Schreij, D., & Theeuwes, J. (2012). OpenSesame: An open-source, graphical experiment builder for the social sciences. *Behavior Research Methods*, *44*(2), 314–324. https://doi.org/10.3758/s13428-011-0168-7

Mayer, A., Schwiedrzik, C. M., Wibral, M., Singer, W., & Melloni, L. (2016). Expecting to See a Letter: Alpha Oscillations as Carriers of Top-Down Sensory Predictions. *Cerebral Cortex*, *26*(7), 3146–3160. https://doi.org/10.1093/CERCOR/BHV146

Miskovic, V., & Keil, A. (2012). Acquired fears reflected in cortical sensory processing: A review of electrophysiological studies of human classical conditioning. *Psychophysiology*, *49*(9), 1230–1241. https://doi.org/10.1111/j.1469-8986.2012.01398.x

Morris, J. ., & Dolan, R. . (2004). Dissociable amygdala and orbitofrontal responses during reversal fear conditioning. *NeuroImage*, *22*(1), 372–380. https://doi.org/10.1016/J.NEUROIMAGE.2004.01.012

Mueller, E. M., Panitz, C., Hermann, C., & Pizzagalli, D. A. (2014). Prefrontal Oscillations during Recall of Conditioned and Extinguished Fear in Humans. *Journal of Neuroscience*, *34*(21), 7059–7066. https://doi.org/10.1523/JNEUROSCI.3427-13.2014

Nasser, H. M., & Delamater, A. R. (2016). The Determining Conditions for Pavlovian Learning. In *The Wiley Handbook on the Cognitive Neuroscience of Learning* (pp. 5–46). John Wiley & Sons, Ltd. https://doi.org/10.1002/9781118650813.ch2

Ojala, K. E., & Bach, D. R. (2020). Measuring learning in human classical threat conditioning: Translational, cognitive and methodological considerations. *Neuroscience & Biobehavioral Reviews*, *114*, 96–112. https://doi.org/10.1016/j.neubiorev.2020.04.019

Panitz, C., Keil, A., & Mueller, E. M. (2019). Extinction-resistant attention to long-term conditioned threat is indexed by selective visuocortical alpha suppression in humans. *Scientific Reports*, *9*(1), 1–9. https://doi.org/10.1038/s41598-019-52315-1

Pascual-Marqui, R. D. (1999). Review of Methods for Solving the EEG Inverse Problem. In *International Journal of Bioelectromagnetism* (Vol. 1, Issue 1). http://www.tut.fi/ijbem

Pascual-Marqui, R. D., Michel, C. M., & Lehmann, D. (1994). Low resolution electromagnetic tomography: a new method for localizing electrical activity in the brain. *International Journal of Psychophysiology*, *18*(1), 49–65. https://doi.org/10.1016/0167-8760(84)90014-X

Phelps, E. A., Delgado, M. R., Nearing, K. I., & LeDoux, J. E. (2004). Extinction Learning in Humans: Role of the Amygdala and vmPFC. *Neuron*, *43*(6), 897–905. https://doi.org/10.1016/j.neuron.2004.08.042

Quirk, G. J., & Mueller, D. (2008). Neural Mechanisms of Extinction Learning and Retrieval. *Neuropsychopharmacology*, *33*(1), 56–72. https://doi.org/10.1038/sj.npp.1301555

Riels, K., Ramos Campagnoli, R., Thigpen, N., & Keil, A. (2022). Oscillatory brain activity links experience to expectancy during associative learning. *Psychophysiology*, *59*(5), e13946. https://doi.org/10.1111/PSYP.13946

Sangha, S., Diehl, M. M., Bergstrom, H. C., & Drew, M. R. (2020). Know safety, no fear. In *Neuroscience and Biobehavioral Reviews* (Vol. 108, pp. 218–230). Elsevier Ltd. https://doi.org/10.1016/j.neubiorev.2019.11.006

Savage, H. S., Davey, C. G., Fullana, M. A., & Harrison, B. J. (2020). Clarifying the neural substrates of threat and safety reversal learning in humans. *NeuroImage*, *207*, 116427. https://doi.org/10.1016/j.neuroimage.2019.116427

Schiller, D., & Delgado, M. R. (2010). Overlapping neural systems mediating extinction, reversal and regulation of fear. *Trends in Cognitive Sciences*, *14*(6), 268–276. https://doi.org/10.1016/J.TICS.2010.04.002

Schiller, D., Levy, I., Niv, Y., LeDoux, J. E., & Phelps, E. A. (2008). From Fear to Safety and Back: Reversal of Fear in the Human Brain. *Journal of Neuroscience*, *28*(45), 11517–11525. https://doi.org/10.1523/JNEUROSCI.2265-08.2008

Sjouwerman, R., & Lonsdorf, T. B. (2019). Latency of skin conductance responses across stimulus modalities. *Psychophysiology*, *56*(4), e13307. https://doi.org/10.1111/psyp.13307

Spaccasassi, C., Zanon, M., Borgomaneri, S., & Avenanti, A. (2022). Mu rhythm and corticospinal excitability capture two different frames of motor resonance: A TMS–EEG co-registration study. *Cortex*, *154*, 197–211. https://doi.org/10.1016/J.CORTEX.2022.04.019

Sperl, M. F. J., Panitz, C., Hermann, C., & Mueller, E. M. (2016). A pragmatic comparison of noise burst and electric shock unconditioned stimuli for fear conditioning research with many trials. *Psychophysiology*, *53*(9), 1352–1365. https://doi.org/10.1111/PSYP.12677

Sperl, M. F. J., Panitz, C., Rosso, I. M., Dillon, D. G., Kumar, P., Hermann, A., Whitton, A. E., Hermann, C., Pizzagalli, D. A., & Mueller, E. M. (2019). Fear Extinction Recall Modulates Human Frontomedial Theta and Amygdala Activity. *Cerebral Cortex*, *29*(2), 701–715. https://doi.org/10.1093/cercor/bhx353

Starita, F., & di Pellegrino, G. (2018). Alexithymia and the Reduced Ability to Represent the Value of Aversively Motivated Actions. *Frontiers in Psychology*, *9*(DEC), 1–11. https://doi.org/10.3389/fpsyg.2018.02587

Starita, F., Garofalo, S., Dalbagno, D., Degni, L. A. E., & di Pellegrino, G. (2022). Pavlovian threat learning shapes the kinematics of action. *Frontiers in Psychology*, *13*, 6336. https://doi.org/10.3389/fpsyg.2022.1005656

Starita, F., Kroes, M. C. W., Davachi, L., Phelps, E. A., & Dunsmoor, J. E. (2019). Threat learning promotes generalization of episodic memory. *Journal of Experimental Psychology: General*, *148*(8), 1426–1434. https://doi.org/10.1037/xge0000551

Starita, F., Làdavas, E., & di Pellegrino, G. (2016). Reduced anticipation of negative emotional events in alexithymia. *Scientific Reports*, *6*(1), 27664. https://doi.org/10.1038/srep27664

Starita, F., Pietrelli, M., Bertini, C., & di Pellegrino, G. (2019). Aberrant reward prediction error during Pavlovian appetitive learning in alexithymia. *Social Cognitive and Affective Neuroscience*, *14*(10), 1119–1129. https://doi.org/10.1093/scan/nsz089

Stemerding, L. E., van Ast, V. A., Gerlicher, A. M. V., & Kindt, M. (2022). Pupil dilation and skin conductance as measures of prediction error in aversive learning. *Behaviour Research and Therapy*, *157*, 104164. https://doi.org/10.1016/J.BRAT.2022.104164

Sutton, R. S., & Barto, A. G. (1998). *Reinforcement Learning: An Introduction*. MIT Press.

Tarasi, L., Trajkovic, J., Diciotti, S., di Pellegrino, G., Ferri, F., Ursino, M., & Romei, V. (2022). Predictive waves in the autism-schizophrenia continuum: A novel biobehavioral model. *Neuroscience & Biobehavioral Reviews*, *132*, 1–22. https://doi.org/10.1016/J.NEUBIOREV.2021.11.006

Ursino, M., Cesaretti, N., & Pirazzini, G. (2022). A model of working memory for encoding multiple items and ordered sequences exploiting the theta-gamma code. *Cognitive Neurodynamics 2022*, 1–33. https://doi.org/10.1007/S11571-022-09836-9

Ursino, M., Cona, F., & Zavaglia, M. (2010). The generation of rhythms within a cortical region: Analysis of a neural mass model. *NeuroImage*, *52*(3), 1080–1094. https://doi.org/10.1016/J.NEUROIMAGE.2009.12.084

Wischnewski, M., Zerr, P., & Schutter, D. J. L. G. (2016). Effects of Theta Transcranial Alternating Current Stimulation Over the Frontal Cortex on Reversal Learning. *Brain Stimulation*, *9*(5), 705–

711. https://doi.org/10.1016/J.BRS.2016.04.011

Yin, S., Bo, K., Liu, Y., Thigpen, N., Keil, A., Ding, M., Crayton Pruitt, J., & Pruitt, C. (2020). Fear conditioning prompts sparser representations of conditioned threat in primary visual cortex. *Social Cognitive and Affective Neuroscience*, 950–964. https://doi.org/10.1093/scan/nsaa122

Zhang, Z., Mendelsohn, A., Manson, K. F., Schiller, D., & Levy, I. (2015). Dissociating Value Representation and Inhibition of Inappropriate Affective Response during Reversal Learning in the Ventromedial Prefrontal Cortex. *Eneuro*, *2*(6), ENEURO.0072-15.2015. https://doi.org/10.1523/ENEURO.0072-15.2015

Author note

The authors would like to thank Giovanni Pastori for his assistance with data collection.

F.S. and G.d.P. are funded under a Bial Foundation Grant for Scientific Research 2020/2021 [Grant Number 47/20]. F.S. G.S. and G.d.P. are funded under the FLAG-ERA JTC 2019 scheme by MUR (CUP J32F20000870001) for the Human Brain Project titled “The Motor way to Decision Making” (MoDeM).

The authors declare no conflict of interest.

Supplementary materials

Results from the right hemisphere

EEG response

A series of 3 (time intervals: 0-2s, 2-4s, 4-6s) x 4 (phases: Acq1, Acq2, Rev1, Rev2) x 2 (type of CS: CS+, CS-) repeated measures analyses of variance (RM ANOVAs) was conducted to assess differences in theta and alpha power at the presentation of CS during each experimental phase.

Theta. Learning curves for the left midcingulate cortex and ventral mPFC. Figure 1 shows the group mean-normalized theta power to CS+ and CS- in the midcingulate cortex and ventral mPFC, averaged across 5-trial subsets, as a function of the experimental phase (acquisition 1 & 2, or reversal 1 & 2). In the midcingulate cortex, greater response to CS+ (compared to CS-) can be seen in all 4 phases. In the ventral mPFC, discrimination between the two CSs is observed only in Reversal 2, with a greater response to CS- (old CS+) than CS+ (old CS-).

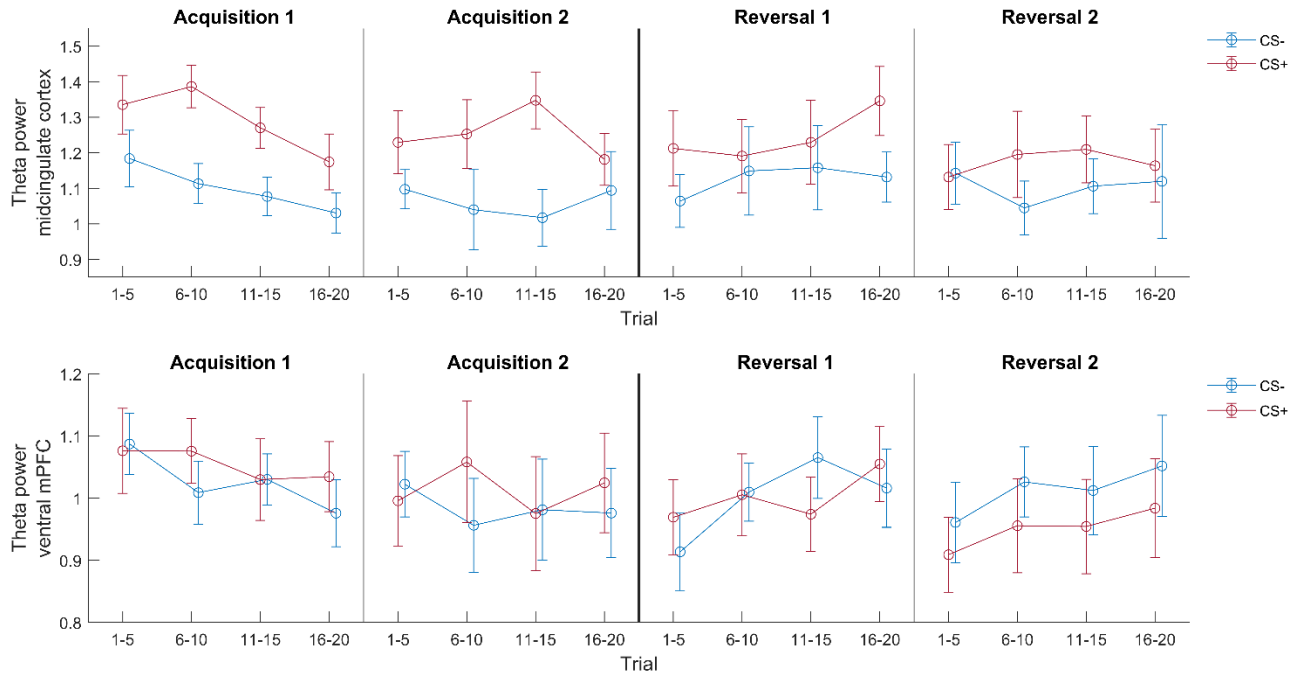

Figure 1. The figure shows group means (white circle) and standard error of the mean (vertical lines) of the normalized theta power (CS+ and CS-) in the [top] midcingulate cortex and [bottom] ventral mPFC, as a function of the experimental phase (acquisition 1 & 2, or reversal 1 & 2) and trial (5 trials subsets mean, 1-5/6-10/11-15/16-20).

Midcingulate cortex. Repeating the analysis of the main text on the right hemisphere replicated the main effect of time (p=.002) and the CS by time interaction (p=.011), with greater power for the CS- than the CS+ in the first 2 sec of CS presentation, while greater power for the CS+ than the CS- in the second and third time intervals of CS presentation. No other main effect or interaction was significant (all $p \geq .356$).

Ventral mPFC. Repeating the analysis of the main text on the right hemisphere showed no significant main effect or interaction (all $p \geq .118$).

Alpha. Learning curves for the left motor and somatosensory cortices. Figure 2 shows the group mean normalized theta power to CS+ and CS- in the motor cortex and somatosensory cortex, averaged

across 5-trial subsets, as a function of the experimental phase (acquisition 1 & 2, or reversal 1 & 2). In all phases, there is a greater response to CS- (compared to CS+), especially in the motor cortex.

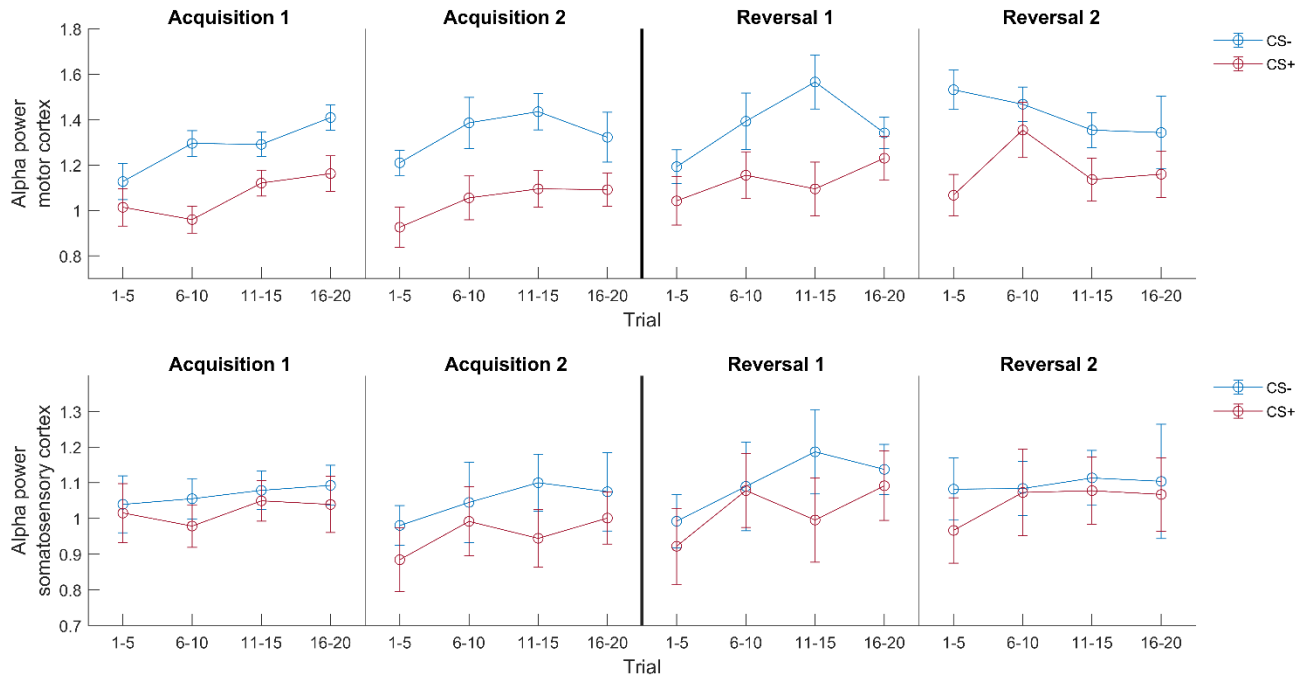

Figure 2. The figure shows group means (white circle) and standard error of the mean (vertical lines) of the normalized alpha power (CS+ and CS-) in the [top] motor and [bottom] somatosensory cortices, as a function of the experimental phase (acquisition 1 & 2, or reversal 1 & 2) and trial (5 trials subsets mean, 1-5/6-10/11-15/16-20).

Motor cortex. Repeating the analysis of the main text on the right hemisphere replicated the main effect of the CS ($p=.015$), with greater power for the CS- than the CS+, and showed a time by phase interaction ($p=.002$). No other main effect or interaction was significant (all $p \geq .356$).

Somatosensory cortex. Repeating the analysis of the main text on the right hemisphere showed no significant main effect or interaction all $p \geq .077$).

Visual cortex. Repeating the analysis of the main text on the right hemisphere showed no significant main effect or interaction (all $p \geq .063$).